



**HAL**  
open science

## **Polyphase tectonic history of the Southern Peninsula, Haiti: from folding-and-thrusting to transpressive strike-slip**

Richard J.F. Wessels, Nadine Ellouz-Zimmermann, Nicolas Bellahsen, Youri Hamon, Claudio L Rosenberg, Rémy Deschamps, Roberte Momplaisir, Dominique Boisson, Sylvie Leroy

### ► To cite this version:

Richard J.F. Wessels, Nadine Ellouz-Zimmermann, Nicolas Bellahsen, Youri Hamon, Claudio L Rosenberg, et al.. Polyphase tectonic history of the Southern Peninsula, Haiti: from folding-and-thrusting to transpressive strike-slip. *Tectonophysics*, 2019, 751, pp.125-149. 10.1016/j.tecto.2018.12.011 . hal-02067833

**HAL Id: hal-02067833**

**<https://hal.science/hal-02067833v1>**

Submitted on 4 Nov 2019

**HAL** is a multi-disciplinary open access archive for the deposit and dissemination of scientific research documents, whether they are published or not. The documents may come from teaching and research institutions in France or abroad, or from public or private research centers.

L'archive ouverte pluridisciplinaire **HAL**, est destinée au dépôt et à la diffusion de documents scientifiques de niveau recherche, publiés ou non, émanant des établissements d'enseignement et de recherche français ou étrangers, des laboratoires publics ou privés.

# **Polyphase tectonic history of the Southern Peninsula, Haiti: From folding-and-thrusting to transpressive strike-slip**

Richard J.F. Wessels<sup>1, 2</sup>, Nadine Ellouz-Zimmermann<sup>2</sup>, Nicolas Bellahsen<sup>1</sup>, Youri Hamon<sup>2</sup>, Claudio Rosenberg<sup>1</sup>, Remy Deschamps<sup>2</sup>, Roberte Momplaisir<sup>3</sup>, Dominique Boisson<sup>3</sup>, Sylvie Leroy<sup>1</sup>

1. Sorbonne Université, CNRS-INSU, Institut des Sciences de la Terre Paris, ITeP UMR 7193, F-75005 Paris, France.
2. IFP Energies nouvelles, IFPE, Geosciences, Rueil-Malmaison, France.
3. Université d'Etat d'Haïti (UEH), Port-au-Prince, Haiti.

## **Abstract**

The Southern Peninsula of Haiti is a seismically active east – west trending transpressive mountain range with elevations over 2 km. Present-day deformation is mainly partitioned along the left-lateral Enriquillo – Plantain Garden Fault Zone (EPGFZ) and associated oblique reverse faults and/or folds. The configuration of these faults, their respective timing, and the role of structural heritage on their development is poorly understood. To address these questions we present the results of extensive field campaigns, combined with satellite imagery interpretation and published data, which allows us to constrain the Cenozoic evolution of the Southern Peninsula. Our results show a polyphase tectonic history consisting of three major tectonic events: 1) Maastrichtian to early Paleocene crustal-scale folding that developed coevally with predominantly north to northeast dipping thrusts, resulting in uplift and erosion of the Cretaceous sedimentary cover in large parts of the Southern Peninsula. 2) Early Miocene uplift and erosion, which was strongest in the southwestern part of the peninsula and

decreased eastwards, did not affect the Massif de la Selle. Uplift is most likely unrelated to strike-slip activity but resulted from folding in response to NE – SW shortening that possibly reactivated older, predominantly N- to NE-dipping thrusts. 3) Late Miocene to present-day deformation and uplift. Spatially distributed strike-slip started during the late Miocene and became progressively focused along the EPGFZ in the latest Miocene. Oblique and thrust faults locally post-date strike-slip activity from the Pliocene onward. Increase in compressional deformation from west to east is reflected by a change in structural style, with predominantly strike-slip faults in the west and transpressional faults in the east, the latter possibly rooted on the EPGFZ at depth. Paleo-stresses associated with a strike-slip regime are at a significantly high angle to the trace of the EPGFZ, indicating that the EPGFZ is a mechanically weak fault.

## **Keywords**

Southern Peninsula Haiti; EPGFZ; folding-and-thrusting; transpressive strike-slip; paleo-stress

## **1. Introduction**

Haiti is located on the western side of the island of Hispaniola and occupies a central position in the northern Greater Antilles arc in the Caribbean (Fig. 1a). The Southern Peninsula of Haiti experienced devastating earthquakes in the past (McCann, 2006; Ali et al., 2008; Bakun et al., 2012). These historical earthquakes occurred proximal to a N80°E trending onshore lineament stretching from Tiburon in the west up to Pétionville in the east (Fig. 1b). This segmented lineament is easily traced on satellite images and is known as the Enriquillo – Plantain Garden Fault Zone (EPGFZ; Mann and Burke, 1984), left-lateral strike-slip system (Fig. 2a; Calmus, 1984; Mann and Burke, 1984; Mann et al., 1995). The seismogenic nature of the Southern Peninsula was once more demonstrated by the Mw 7.0 2010 Leogâne earthquake that struck 30 km west of the capital of Port-au-Prince (Hayes et al., 2010; Bilham, 2010).

This event likely did not involve surficial slip along the steeply south-dipping EPGFZ segment in this region (Prentice et al., 2010), but resulted from oblique slip on the NNW-dipping blind Leogâne fault (Calais et al., 2010; Mercier de Lépinay et al., 2011; Douilly et al., 2013). Aftershocks also indicate reverse motion along a SSW-dipping fault (Symithe et al., 2013) that coincides with the offshore Trois Baies fault (Fig. 2a; Bien-Aime Momplaisir, 1986). The transpressive nature of this fault system is shown by GPS velocity models in this region (Fig. 1b; Benford et al., 2012a; Calais et al., 2016). The geometry, characteristics, timing, and pre-Holocene stress history of the fault systems in southern Haiti remains poorly understood.

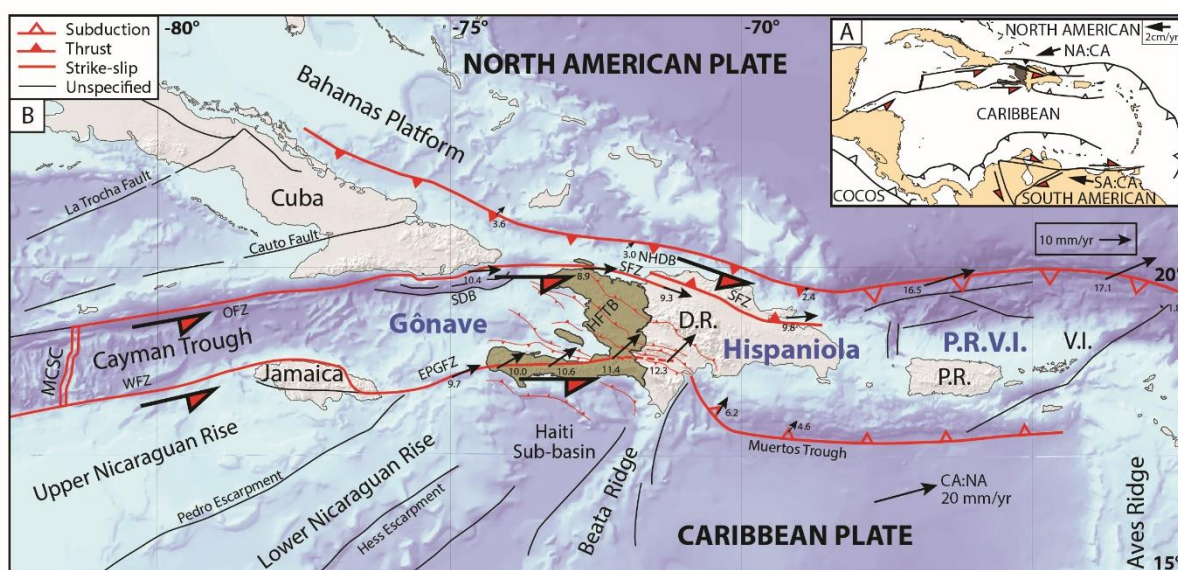


**Fig. 1a:** Geodynamic setting of the Caribbean. GPS velocities (black arrows) from DeMets et al. (2010) in a Caribbean reference frame. **Fig. 1b:** Geodynamic setting of Haiti. GPS velocity vectors (black arrows) from Calais et al. (2016). GPS velocity vectors indicate motion of block to the south (west) of fault with respect to block to the north (west). Faults modified after Leroy (1995). MCSC = Mid-Cayman Spreading Center; OFZ = Oriente Fault Zone; SDB = Santiago Deformed Belt; SFZ = Septentrional Fault Zone; NHDB = North Hispaniola Deformed Belt; HFTB = Haitian Fold-and-thrust belt; EPGFZ = Enriquillo-Plantain Garden Fault Zone; WFZ = Walton Fault Zone; D.R. = Dominican Republic; P.R. = Puerto Rico; V.I. = Virgin Islands; PRVI = Puerto Rico – Virgin Islands block.

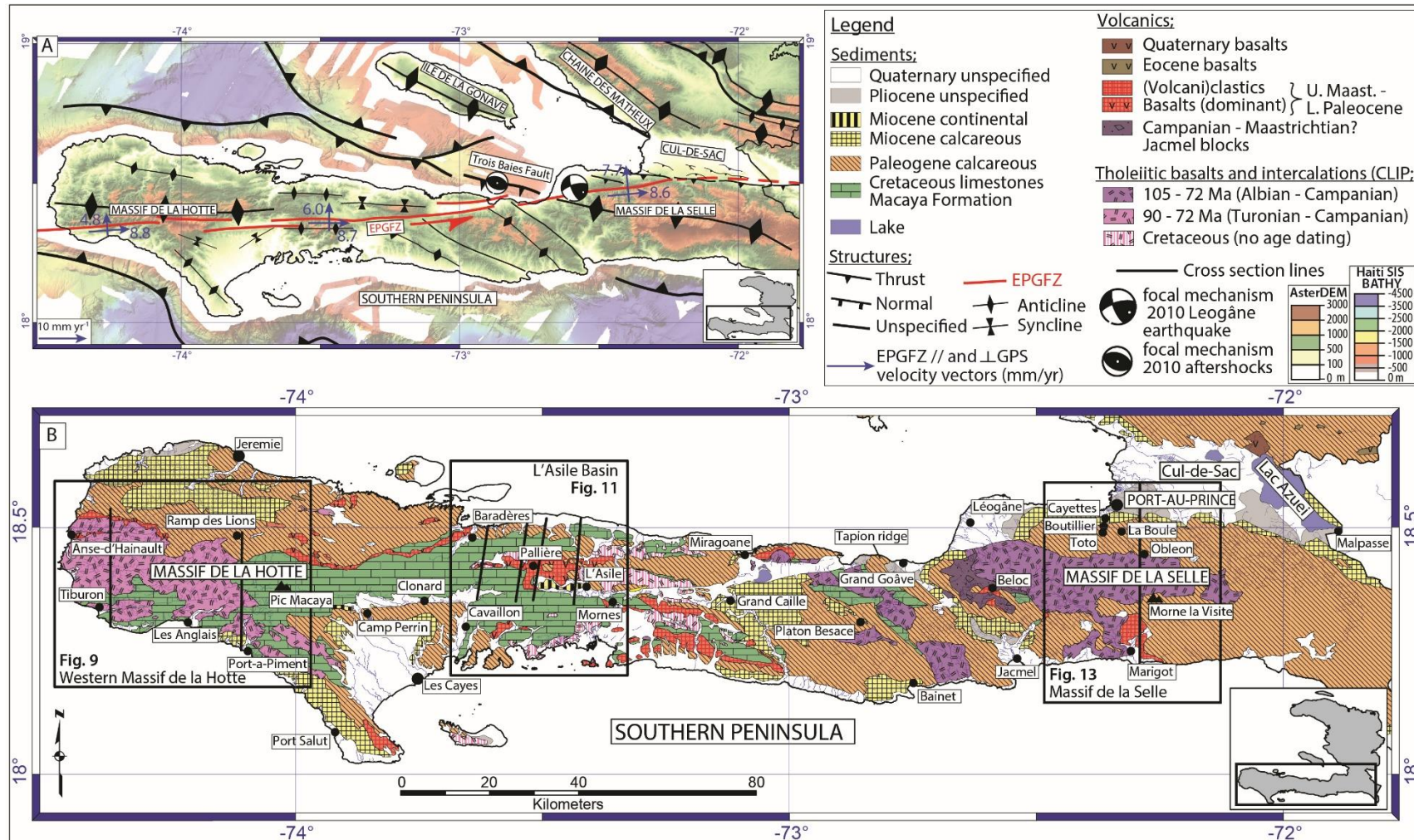
The number of deformation phases that affected the Southern Peninsula during the Cenozoic era, the geographic extent of these phases, and the timing and configuration of the associated faults is also still subject to debate. Previous studies on the geology of the Southern Peninsula note the possibility of a Maastrichtian to Paleocene deformation phase affecting the region (Mercier de Lépinay et al., 1979; Calmus, 1983; Van den Berghe, 1983a; Bien-Aime Momplaisir, 1986; Calmus and Vila, 1988), while others propose tectonic quiescence during this period (Maurrasse, 1982; Desreumaux (1987), in

Bourgueil et al., 1988; Amilcar, 1997). Similar disagreement exists about whether or not an earliest Miocene deformation phase did (Calmus, 1983; Van den Berghe, 1983a; Bizon et al., 1985; Bien-Aime Momplaisir, 1986) or did not (Desreumaux, 1985a, 1987; Bourgueil et al., 1988) affect the southern Peninsula and if it is related to strike-slip activity along the EPGFZ (Calmus, 1983; Bizon et al., 1985; Calmus and Vila, 1988). The configuration, timing, and origin of deformation and faulting in the eastern Southern Peninsula and Cul-de-Sac plain are also subject to debate (Fig. 2a). Some authors argue in favor of a continuation of the EPGFZ into the Cul-de-Sac Plain and Enriquillo Valley in the Dominican Republic (Mann et al., 1995; Wang et al., 2018) while others propose that active thrust faults along the southern border of the Cul-de-Sac truncate the EPGFZ (Bourgueil et al., 1988; Symithe and Calais, 2016), or that normal faulting dominates the southern border (Pubellier et al., 2000).

The aim of this paper is to understand the structural evolution of the Southern Peninsula during the Cenozoic era and the temporal and spatial evolution of the EPGFZ and associated faults. Of particular interest are the next questions: 1) how many episodes of deformation has the Southern Peninsula experienced during the Cenozoic, 2) what was the structural style associated with the successive deformation phases, and 3) how are paleo-stresses distributed and oriented along the EPGFZ and what is their timing?

Three study areas are selected, based on results from field campaigns conducted in 2014, 2015, and 2017. These are the western Massif de la Hotte, l'Asile Basin, and Massif de la Selle regions of the Southern Peninsula (Fig. 2b). Detailed mapping of these three areas is based on the interpretation of satellite imagery, which is controlled and tested against field data. Stratigraphic columns derived from literature are updated with field observations and serve as a first-order constraint for our cross sections. Paleostresses are deduced from the inversion of fault kinematic slip data obtained at outcrops. The before mentioned data allows us to present a coherent structural model for the evolution of the Southern Peninsula, which shows a polyphase tectonic history with deformation phases in the latest Cretaceous - Paleocene, early Miocene, and late Miocene – present-day.





1 **Fig. 2a:** Structural map of the Southern Peninsula. Onshore shaded relief is 30m resolution ASTER DEM, offshore bathymetry is at 25m resolution and was collected during  
 2 the Haiti-SIS cruises (Leroy et al., 2015). Offshore faults from Bien-Aime Momplaisir (1986) and Leroy et al. (2015). Onshore structures from Mann et al. (1995), Saint Fleur et  
 3 al. (2015), Symithe and Calais (2016). Dashed trace of EPGFZ represents interpretation by Wang et al. (2018). GPS velocity vectors constructed from Calais et al. (2016).  
 4 Earthquake focal mechanisms from the International Seismological Centre (2014) (GCMT). **Fig. 2b:** Compilation and simplification of 1:250.000 geological maps published by  
 5 the Bureau des Mines et de l'Energie d'Haïti (BME) after Boisson and Bien-Aime Momplaisir, 1987; Bien-Aime Momplaisir et al., 1988). Black rectangles show extent of small  
 6 scale geological maps and corresponding figures. Black lines are cross sections.

## **2. Geological setting**

### **2.1 Geodynamic setting**

Haiti is located in a geodynamically complex area, at the boundary between the North American and Caribbean plates (Fig. 1a). This boundary zone comprises an amalgamation of microplates and blocks bounded by fault zones (Fig. 1b; Benford et al., 2012a; Calais et al., 2016).

The northern plate boundary between the Gonâve and North American plates is defined by the left-lateral Oriente Fault Zone (OFZ), which passes through the Santiago Deformed Belt (SDB) south of Cuba to link up with the Septentrional Fault Zone (SFZ) in Hispaniola (Fig. 1b; Heubeck and Mann, 1991; Calais and Mercier de Lépinay, 1995). The boundary between the Gonâve and Hispaniola blocks possibly corresponds to the northeastern boundary of the Haitian fold-and-thrust belt (Fig. 1b; Benford et al., 2012a; Symithe et al., 2015), which is a southwest-verging, forward propagating thrust system (Pubellier et al., 2000). The southern boundary between the Gonâve microplate and the Caribbean plate coincides with the Walton Fault Zone (WFZ) - Enriquillo-Plantain Garden Fault Zone (EPGFZ) system (Fig. 1b; Benford et al., 2012a; Symithe et al., 2015). In the west, the WFZ marks the southern border of the Cayman Trough (Rosencrantz and Mann, 1991; Leroy et al., 2000), which is connected with the EPGFZ through Jamaica (Benford et al., 2015). East of Jamaica the EPGFZ crosses the Jamaica Passage (Leroy et al., 2015; Corbeau et al., 2016a) and continues onshore the Southern Peninsula (Duplan, 1975; Calmus, 1983; Van den Berghe, 1983b; Mann et al., 1995; Prentice et al., 2010). In the eastern Southern Peninsula (Fig. 2a) the EPGFZ either continues through the Cul-de-Sac plain (Mann et al., 1995; Wang et al., 2018) or is abutting against E- to ESE-trending thrust faults (Saint Fleur et al., 2015; Symithe and Calais, 2016).

Present-day deformation along the northern Caribbean plate boundary changes from almost pure strike-slip along the WFZ and the Jamaica Passage in the west (Benford et al., 2012a; Leroy et al., 2015; Symithe et al., 2015; Corbeau et al., 2016b), to increasingly more transpressive along the EPGFZ in the Southern Peninsula in the east (Ali et al., 2008; Calais et al., 2016).

## ***2.2 Stratigraphy of the Southern Peninsula***

The distribution of the formations described below is found on 1:250.000 geological maps (Published by the Bureau des Mines et de l'Energie d'Haïti (BME) after Boisson and Bien-Aime Momplaisir, 1987; Bien-Aime Momplaisir et al., 1988), which are simplified and presented in Fig. 2b. The purpose of this section is to describe the general stratigraphy of the Southern Peninsula. A corresponding schematic stratigraphic column is presented in Fig. 3. A detailed discussion of our stratigraphic observations is given in section 4.

The oldest rocks exposed on the Southern Peninsula are Cretaceous in age and composed of an alternation of tholeiitic basalts, limestones and radiolarites (Fig. 3; Dumisseau Formation of Maurrasse et al., 1979). The lowermost part contains Aptian – Albian rudists indicative of platform facies (Bien-Aime Momplaisir, 1986; Bourgueil et al., 1988). Laterally and upwards in the stratigraphy pelagic facies dominate until late Campanian times (Maurrasse et al. (1979), Desreumaux (1987), in Bourgueil et al., 1988; Mann et al., 1991; Amilcar, 1997). The thickness of this basaltic complex is at least 1500m (Bourgueil et al., 1988), with a similar thickness estimated offshore using seismic refraction (Mauffret and Leroy, 1997) and submersible sampling (Mauffret et al., 2001). This succession is part of the Caribbean Large Igneous Province (CLIP) that extruded in a submarine setting (Sinton et al., 1998; Kerr et al., 2003). The Cretaceous sedimentary cover corresponds to the calcareous Macaya Formation of Butterlin (1954), which is also found in the Caribbean offshore (Kroehler et al., 2011). Onshore the Southern Peninsula it consists of well stratified pelagic limestones with chert nodules and occasional claystone and radiolarite beds deposited under bathyal conditions (Calmus, 1983). The age of this formation is well constrained from Campanian to middle Maastrichtian, although the base could be located in the Coniacian (Ayala, 1959; Maurrasse, 1982; Calmus, 1983; Van den Berghe, 1983; Desreumaux (1987), in Bourgueil et al., 1988). The facies indicate a general deepening of the depositional environment throughout the Late Cretaceous.



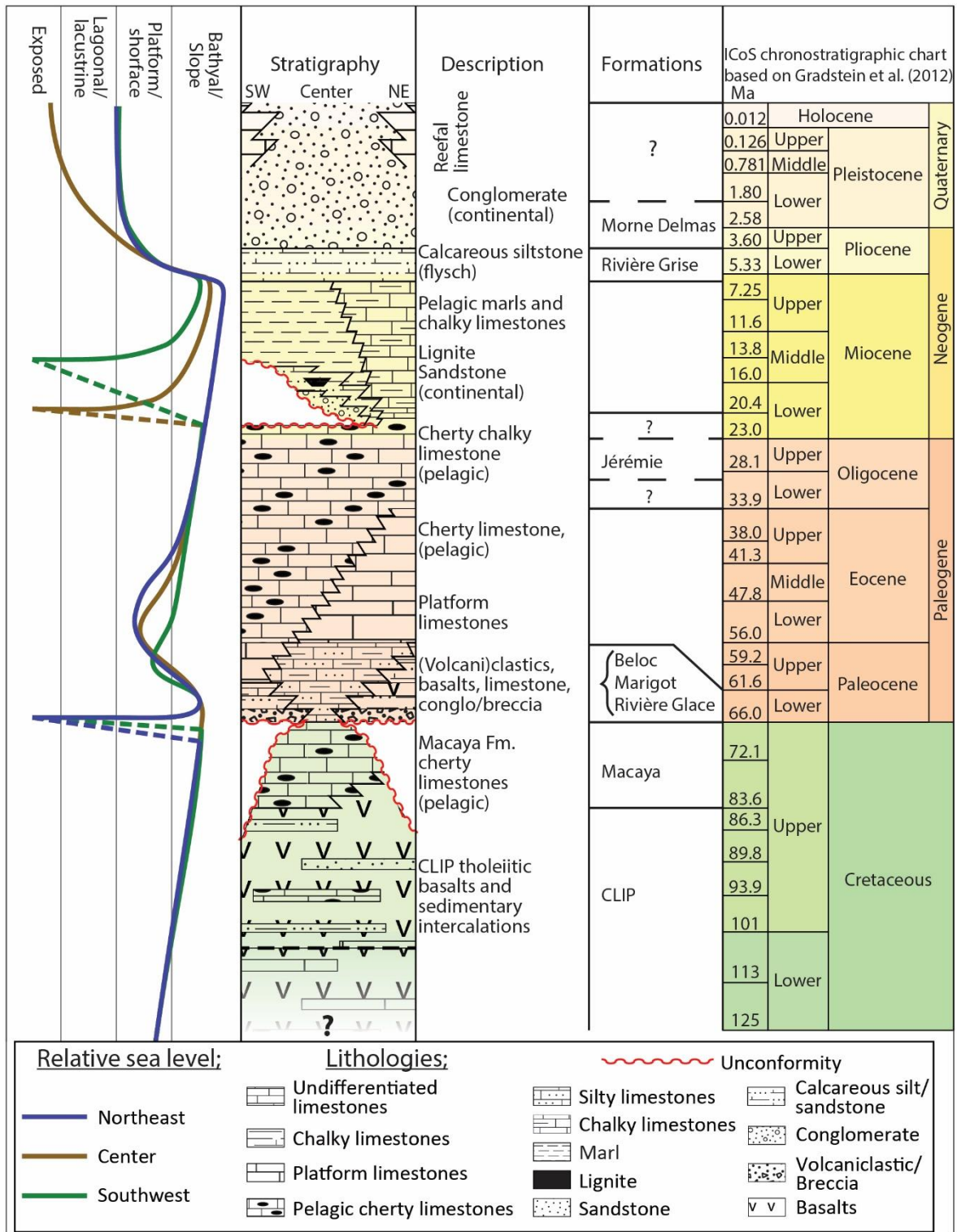


**Fig. 3:** Synthetic stratigraphic column for the Southern Peninsula. Relative sealevel for northeast (blue), central (brown) and southwest (green). Data from references in text. Chronostratigraphic chart from the International Commission on Stratigraphy (ICoS) based on the geologic time scale from Gradstein et al. (2012).

The Cretaceous basalts and limestones are unconformably overlain by a diachronous transgressive fining-upwards sequence that becomes more calcareous through time (Bourgueil et al., 1988). This Paleocene sequence commences with shallow water conglomerates and volcanoclastic breccias, clay-silt- and sandstones overlain by turbiditic silty limestones (Van den Berghe, 1983a; Bourgueil et al., 1988; Amilcar, 1997), and locally possibly platform limestones (Calmus, 1983). The Paleocene sequence is occasionally interbedded with transitional to calc-alkaline basalts (Calmus, 1987). The temporal and lateral equivalents of the Paleocene detrital series on the Southern Peninsula are known by the following formation names; Marigot in the south-east (Butterlin, 1960), Beloc in the central-east (Desreumaux, 1987) and Rivière Glace in the west (Calmus, 1983). Locally the transition from Maastrichtian to Paleocene is conformable or characterized by an upper Maastrichtian ravinement surface (Desreumaux, 1985b; Bourgueil et al., 1988), or by K-T impact ejecta material (Maurrasse and Sen, 1991).

The Eocene is characterized by deeper depositional facies on the southernmost part of the peninsula compared to the northern part (Desreumaux, 1985a). In the north, lower Eocene platform limestones rich in benthic foraminifera progressively change to middle to upper Eocene outer platform limestones (Calmus, 1983). In the southernmost part the Eocene stratigraphy is dominated by cherty pelagic slope limestones (Bourgueil et al., 1988). Calc-alkaline basalts interbedded in lower to middle Eocene limestones are observed in the western part of the Southern Peninsula (Calmus, 1987).

The Oligocene through late Miocene facies are characterized by deep marine chalks with cherts, pelagic mudstones, chalky limestones and marls (Maurrasse, 1980; Van den Berghe, 1983; Desreumaux (1987), in Bourgueil et al. 1988). Local highs represented by platform facies are also observed (Bien-Aime Momplaisir, 1986). A notable exception to these submarine depositional environments is found west of Camp Perrin in the west-central part of the Southern Peninsula (Fig. 2b). Fining upwards detrital deposits of Burdigalian to Langhian age commence with basal littoral conglomerates containing Cretaceous basalts and limestones pebbles, which are overlain by lacustrine

sands and clays interbedded with lignite levels (Calmus, 1983). The age of these deposits is disputed by Bourgueil et al. (1988) who argued that the sediments could be reworked and therefore much younger. The detrital series possibly has a lateral equivalent in the L'Asile region (Fig. 2b; Bien-Aime Momplaisir, 1986), although in this basin the age is less well constrained. The implication of these littoral and lagoonal facies on the Miocene evolution of the Southern Peninsula are further addressed in the discussion.

The late Miocene marks a change in depositional environment. Pelagic limestones and marls are progressively overlain by flysch-type detrital deposits, whose facies display a shallowing upwards trend from the late Messinian onwards (Maurrasse, 1982; Bourgueil et al., 1988). The detrital feldspar fraction in Pliocene deposits consists of labradorite that signals erosion and sourcing from CLIP-type basalts in the area (Bizon et al., 1985; Desreumaux, (1987), in Bourgueil et al., 1988). A similar facies change occurred during the late Miocene to Pliocene in the Enriquillo Basin in the Dominican Republic (Mann et al., 1991b; McLaughlin and Sen Gupta, 1991; Díaz de Neira, 2002). Quaternary continental facies were deposited in basins along-strike and proximal to the trace of the EPGFZ, and in the Les Cayes, Leogâne and Cul-de-Sac basins (Fig. 2b), while reefal platform limestones were confined to the coastal areas (Mann et al., 1995).

### **2.3 Tectonic evolution of the Southern Peninsula during the Cenozoic**

The existence and effects of a Late Cretaceous to Paleocene tectonic event on Haiti's Southern Peninsula is still subject to debate. Authors in favor such a deformation event (Mercier de Lépinay et al., 1979; Calmus, 1983; Van den Berghe, 1983a; Bien-Aime Momplaisir, 1986; Calmus and Vila, 1988) note: (1) the presence of an angular unconformity between the Paleocene and Cretaceous formations, (2) the existence of deformed Cretaceous limestone fragments in olistoliths encountered in the Paleocene Rivière Glace formation, (3) outcrop-scale isoclinal folding of the Cretaceous Macaya limestone with a vergence towards the NE, (4) Cretaceous Macaya limestones thrust over lower

Paleocene detrital deposits, both of which are unconformably covered by upper Paleocene limestones, (5) a difference in fold-wavelength and deformation intensity between the Cretaceous units and post-Paleocene sediments. Other authors (Maurrasse, 1982; Desreumaux, 1985b; Bourgueil et al., 1988; Amilcar, 1997) disagree with this interpretation, and argue that: (1) the transition from Cretaceous to Paleocene is conformable and (2) the observed deformation results only from Neogene tectonics. The latter would imply that the difference in fold-wavelength between the Cretaceous and Cenozoic units is caused by: (i) differences in the mechanical response of the two units to folding, (ii) proximity to Neogene tectonic structures or (iii) a combination of both.

Angular unconformities of early Miocene age are locally observed in the southwestern (Calmus, 1983; Amilcar, 1997), central (Bien-Aime Momplaisir, 1986) and eastern (Van den Berghe, 1983a) Southern Peninsula. The importance, geographical extent, and even existence of these unconformities is disputed by Desreumaux (1985b) and Bourgueil et al. (1988). A widespread homogenization of pelagic sedimentation marks a phase of tectonic quiescence during the middle to late Miocene (Bourgueil et al., 1988). The latest phase of uplift of the Southern Peninsula started during the late Miocene with erosion reaching the Cretaceous basalts from the late Messinian onwards (Bizon et al., 1985; Bourgueil et al., 1988).

The most dominant structural feature on the Southern Peninsula is the N080°E trending Tiburon – Pétionville lineament (Duplan, 1975), known as the Enriquillo-Plantain Garden Fault Zone (EPGFZ) (Fig. 2a; Mann et al., 1984; Mann et al., 1995). Present-day activity of this left-lateral fault is documented by: 1) Quaternary sedimentation within subsiding pull-apart basins along its trace, most notably the Miragoane, Clonard and smaller unnamed basins in the Tiburon Valley (Mann et al., 1983), 2) left-lateral offset of Quaternary alluvium (Mann et al., 1995) and stream channels (Prentice et al., 2010), and 3) folded Quaternary sediments north of Camp Perrin that are part of a restraining bend that causes uplift in the area around Pic Macaya (Mann et al., 1995). The timing of onset of strike-slip

activity on the Southern Peninsula is still debated (Wessels, 2019), with ages ranging from the Eocene (Calmus, 1984) to the Pliocene (Bourgueil et al., 1988; Mann et al., 1995; Symithe and Calais, 2016).

### 3. Methodology

Biostratigraphic data from literature (Calmus, 1983; Van den Berghe, 1983a; Bien-Aime Momplaisir, 1986; Bourgueil et al., 1988; Amilcar, 1997) was used to create compilation maps that highlight the Maastrichtian – early Paleocene (Fig. 4a) and early Miocene (Fig. 4b) unconformities. None of the above literature provides coordinates for sample sites, but rather specifies sample locations relative to a village, road, river, or cross section. Although care has been taken to re-localize the samples, their location as presented in Fig. 4a and Fig. 4b should be viewed with caution. Taxa quoted in the publications was checked against the Mikrotax database and placed in the correct nannofossil (Young et al., 2018a) and planktonic (Young et al., 2018b) zones. The planktonic taxa were cross-checked, when possible, against the data provided in BouDagher-Fadel (2015), while the benthic taxa were checked against the data in BouDagher-Fadel (2008), unless otherwise stated. The extended compilation of data can be found in Appendix 1 for the Maastrichtian - early Paleocene and Appendix 2 for the early Miocene unconformities. The correlation between the planktonic, benthic, or nannofossil and the geologic time scale is after Hilgen et al. (2012) for the Neogene, Vandenberghe et al. (2012) for the Paleogene and Ogg et al. (2012) for the Cretaceous periods.

We re-mapped three parts of the island (Fig. 9, Fig. 11 and Fig. 13) based on field observations combined with satellite imagery. These maps contain a reference grid with 0.1° spacing. Background shaded relief is obtained from ASTER DEM. Elevation contour lines with 50m are from the Haitian Centre National de l'Information Géo-Spatiale (CNIGS). These contours are slightly shifted to match the DEM and the course of rivers although the fit is not perfect. Offshore bathymetry contours are from GEBCO, with the first two contour lines at 50m increment and all deeper contours at 250m increment. The geological maps were created using a workflow (Appendix 3) involving: 1) implementation of stratigraphic and structural data derived from literature supplemented with our field observations, 2) georeferenced mapping with MAPublisher® using the DEM and elevation



contours, 3) exportation and transparent overlay of the mapped units in Google Earth® for quality control, and 4) re-iteration of the above steps to arrive at the final result.

Stratigraphic columns used to guide the geological mapping and the cross sections can be found in Appendix 4, whose locations are displayed on the cross sections of Fig. 10, Fig. 12 and Fig. 14. The formation name, age, lithology, depositional environment, thickness, and associated references can be found in Appendix 5.

Kinematic fault slip data was analyzed using the multiple inverse software package from Yamaji et al. (2005). The orientation of shear fractures (sensu Twiss and Moores, 2007; Fossen, 2010) and the sense and orientation of kinematic indicators such as slickenlines (i.e. striations, ridges, grooves), slickenfibres (i.e. calcite steps) and slickolites on these fracture planes are used as input parameters for the program. The numerical inversion method allows separation of different paleostress states from heterogeneous fault slip data. The fault dataset and obtained reduced stress tensor were back-tilted to obtain an Andersonian configuration (Anderson, 1905) for the stress states, with one stress axis perpendicular and two parallel to the earth's surface. When present, we used the strike of the bedding to guide the back-tilting. If back-tilting the stress state using the bedding as a guiding plane did not result in an Andersonian configuration, the original dataset was preserved. Even though faults and shear fractures can form in non-Andersonian configurations, for instance resulting from topographic effects, heterogeneities within the rock, great depth of initiation, or zones of weakness (Simpson, 1997), an Andersonian configuration offers good first-order constraints for analyzing the data. Any stress inversion results that, in their present setting, deviate strongly from an Andersonian configuration are discussed separately.

## 4. Results

### 4.1 Maastrichtian – early Paleocene unconformity

The compilation map of biostratigraphic data for the Maastrichtian – early Paleocene unconformity based on the work by Mercier de Lépinay et al. (1979), Calmus (1983), Van den Berghe (1983), Bien-Aime Momplaisir (1986), Bourgueil et al. (1988) and Amilcar (1997) is presented in Fig. 4a, while an extensive overview can be found in Appendix 1. The Campanian to Maastrichtian (Ayala, 1959; Maurrasse, 1982; Calmus, 1983; Van den Berghe, 1983a; Desreumaux, 1985b) Macaya Formation is eroded in the western Massif de la Hotte, the eastern l'Asile region and in large parts of the Massif de la Selle (Fig. 4a). In these areas, for instance west of Morne la Visite in the Massif de la Selle (Fig. 2b), the Cretaceous CLIP basalts are unconformably overlain by lower Paleocene conglomerates and clastics containing erosional products derived from the Cretaceous basalts and Macaya Formation (Fig. 5a; Calmus, 1983; Bourgueil et al., 1988). The sequence generally displays a deepening and fining upwards trend and becomes more calcareous upwards in the sequence (Calmus, 1983; Van den Berghe, 1983a; Bien-Aime Momplaisir, 1986; Amilcar, 1997). In the eastern Massif de la Hotte and western Massif de la Selle (Fig. 4a) the Macaya Formation is not completely eroded and the contact with the lower Paleocene is marked by a ravinement surface (Desreumaux, 1985b; Bourgueil et al., 1988) or a minor erosional unconformity (Calmus, 1983; Van den Berghe, 1983a). Even though the lower Paleocene is directly overlying the Macaya Formation in these areas, the uppermost Maastrichtian is never observed in-situ and only found as erosional products (Bourgueil et al., 1988). Because of the lithological homogeneity (Bourgueil et al., 1988) and similarity in facies (Calmus, 1983) of the Macaya Formation throughout the Southern Peninsula, it is unlikely that the absence of this formation in certain areas can be ascribed to local non-deposition. It is more likely that the Macaya Formation was deposited throughout the Southern Peninsula during the Campanian to Maastrichtian and locally became uplifted and eroded.

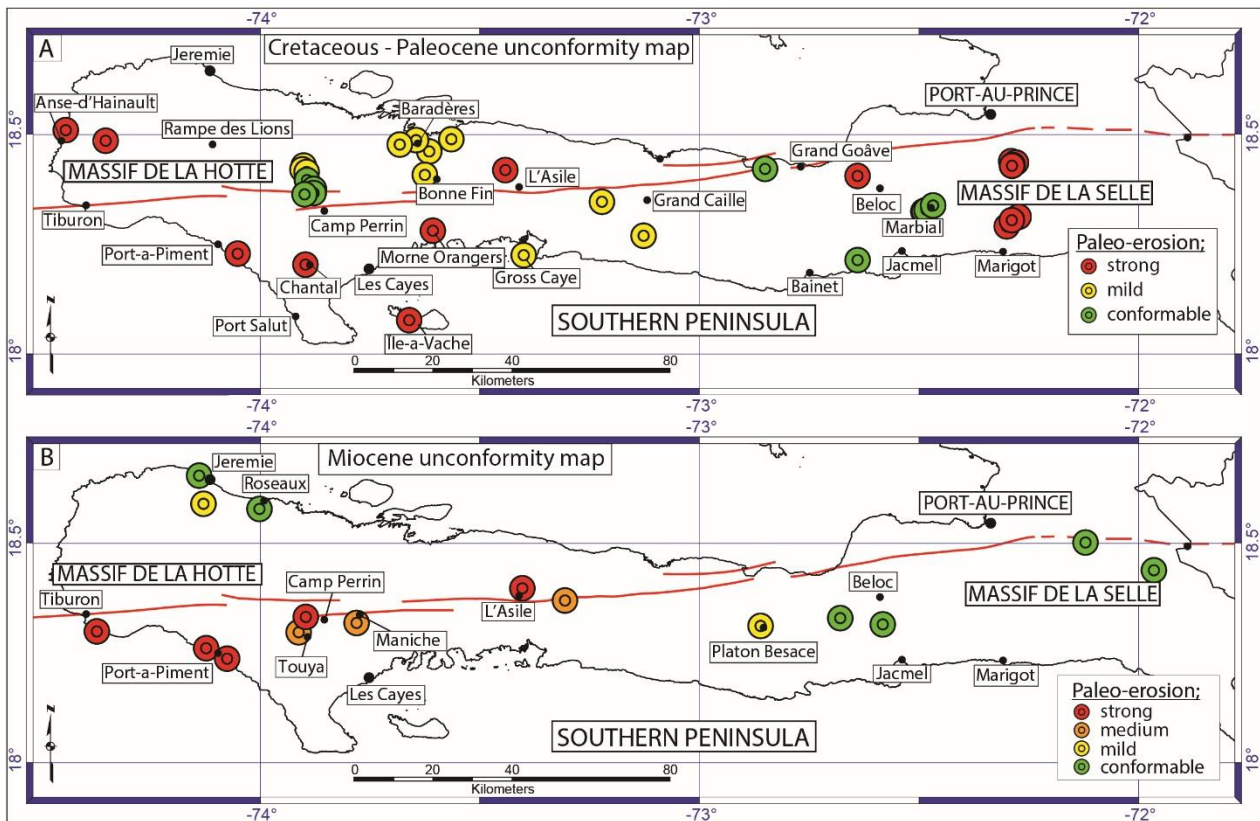


**Fig. 4a:** Compilation map of the Cretaceous – Paleocene unconformity based on biostratigraphic ages for Paleocene deposits and underlying formations. Color coding indicates paleo-erosion. Red; strong, paleo-erosion down into Cretaceous basalts. Yellow; mild, paleo-erosion down into Cretaceous Macaya Formation limestones. Green; conformable, biostratigraphically complete and concordent transition from Cretaceous to Paleogene. **Fig. 4b:** Compilation map of the Cretaceous – Paleocene unconformity based on biostratigraphic ages for lower to middle Miocene deposits and underlying formations. Color coding indicates paleo-erosion. Red; strong, paleo-erosion down to Cretaceous. Orange; medium, paleo-erosion down to Paleocene or Eocene. Yellow; mild, paleo-erosion down to Oligocene or intra-Miocene. Green; conformable, biostratigraphically complete and concordent transition from Paleogene to Neogene. Present-day trace of the EPGFZ on both figures indicated in red. Dashed line represents interpretation by Wang et al. (2018).

## 4.2 Early Miocene unconformity

The compilation map of biostratigraphic data for the early Miocene unconformity based on the work by Calmus (1983), Van den Berghe (1983), Bien-Aime Momplaisir (1986), and Amilcar (1997) is presented in Fig. 4b, while an extensive overview can be found in Appendix 2. Uplift and erosion during the late Oligocene to early Miocene affected the central part of the Southern Peninsula along an E – W trending axis (Fig. 4b). This erosion was strongest at Tiburon where it removed some 1000m of Paleogene cover and cut down into the Cretaceous basalts (Fig. 5b). Intensity of erosion gradually diminishes eastwards towards Maniche. Erosion around l’Asile was again severe and removed around 500 to 1000m of Paleogene sedimentary cover. In the Massif de la Selle only minor nonconformities exist, with the Oligocene to Miocene mostly biostratigraphically complete. The northernmost region of the Massif de la Hotte is unaffected by erosion, with continuous sedimentation spanning the Oligocene and Miocene.

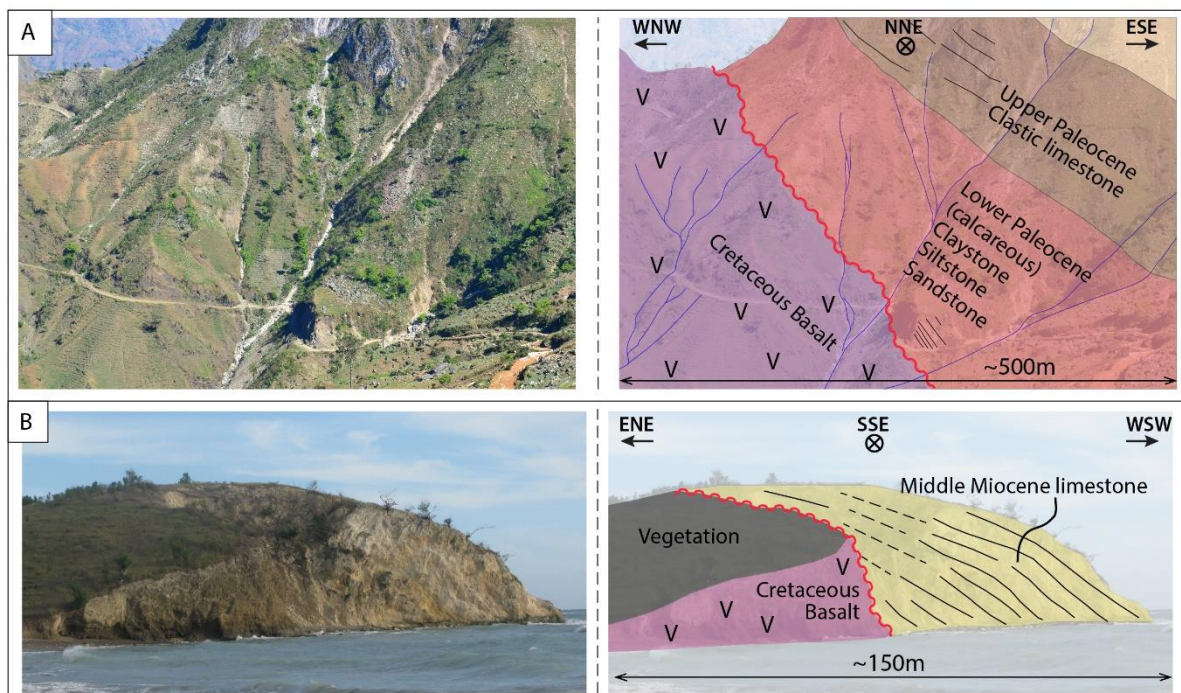


**Fig. 5a:** Unconformable contact between CLIP basalts and calcareous clay-, silt- and sandstones of the lower Paleocene, overlain by upper Paleocene clastic limestones. Top of ridge consists of lower Eocene cherty limestones. Fig. 9; northwest of Morne La Visite. **Fig. 5b:** Unconformable contact between CLIP basalts and middle Miocene limestones. Haut Fort, south of Tiburon.

The areas unaffected by this uplift phase experienced continued sedimentation of deep marine chinks and limestones during early Miocene times (Van den Berghe, 1983a; Bizon et al., 1985; Desreumaux, 1987). The regions affected by the uplift experienced a rapid return to deep marine sedimentation during the middle Miocene. This is characterized by a homogenization of deep marine facies without detrital erosional products that are found throughout the Southern Peninsula in Haiti (Calmus, 1983; Van den Berghe, 1983a; Bizon et al., 1985; Bien-Aime Momplaisir, 1986; Desreumaux, 1987; Bourgueil et al., 1988; Amilcar, 1997), which are similar to the middle Miocene Sombrerito Formation in the eastern Enriquillo Valley in the Dominican Republic (McLaughlin and Sen Gupta, 1991; Díaz de Neira, 2002). The fact that these marine deposits are presently emerged requires another, post-middle Miocene, phase of uplift and erosion.

### ***4.3 Structural style of deformation***

#### **4.3.1 Western Massif de la Hotte**

The Cretaceous basalts and limestones are strongly fractured and folded. Northwest of Les Anglais (Fig. 2b) a 500 x 200 x 100m block of silicified limestones and radiolarites forms a wedge within the Cretaceous basalts. Limestone intercalations within these basalts are boudinaged (Fig. 6a). Halfway Tiburon and Les Anglais (Fig. 2b), blocks of Macaya limestone are embedded as tectonic lenses within the basalts, with intra-basalt faults thrusting folded silicified limestones and radiolarites over Cretaceous basalts with top-to-N motion. In the Tiburon Valley (Fig. 2b), Macaya Formation limestones developed tight disharmonic folds along WNW-trending axes (Fig. 6b).

Eocene platform limestones in this valley are gently folded along W-trending axes (Fig. 6c). The Eocene limestones north of Rampe des Lions (Fig. 2b) are also characterized by gentle to open folds along WNW-trending axes. The Miocene to Quaternary sediments between Port-a-Piment and Tiburon (Fig. 2b) are tilted 35° to the west and are transected by N – S trending normal faults (Fig. 6d).



The Cretaceous formations are more strongly deformed than the Eocene and younger formations, irrespective of their position relative to the EPGFZ. Similar structural observations were made by Calmus (1983) and Amilcar (1997) in this region.

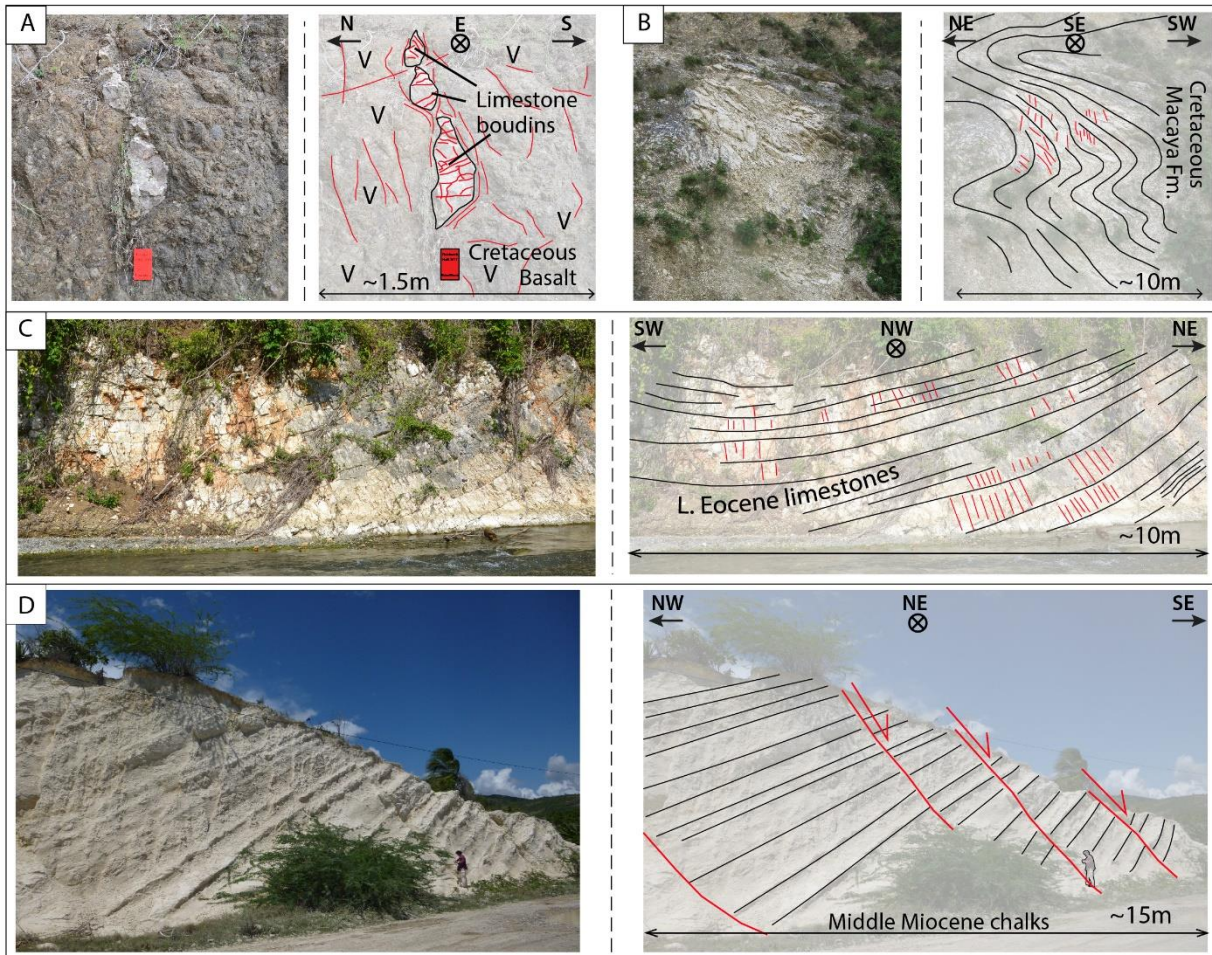


**Fig. 6a:** Boudinage of intercalated limestones within CLIP basalts. Location on Fig. 9; northwest of Les Anglais. **Fig. 6b:** Disharmonically folded Macaya Formation limestones with WNW-trending fold axes. Location on Fig. 9; Tiburon Valley. **Fig. 6c:** Lower Eocene platform limestone gently folded along ENE-trending fold axis. Location on Fig. 9; Tiburon Valley. **Fig. 6d:** North – south trending normal faults in middle Miocene chalks. Location on Fig. 9; NW of Port-a-Piment.

#### 4.3.2 L'Asile region

Southeast of Cavillon (Fig. 2b) the Macaya Formation limestones are folded along a SE-trending axis with a vergence towards the SW. At Mornes (Fig. 2b) a 35° NE dipping thrust separates Macaya limestones from Cretaceous basalts (Fig. 7a). Further southeast along the road tightly folded SW-



verging Paleocene clastic limestones are SW-verging (Fig. 7b). North of Pallière (Fig. 2b) Paleocene clastics and limestones are also folded along ESE-trending axes. The dominant direction of vergence for the Cretaceous and Paleocene formations is towards the south or southwest.

This structural style of deformation differs from the Eocene limestones observed west of Cavillon, which are gently folded along SE- to E-trending axes. Around 9 km east of Camp Perrin, south of Clonard (Fig. 2b), Calmus (1983) observed Eocene to Oligocene mudstones gently folded along N130°E axes.

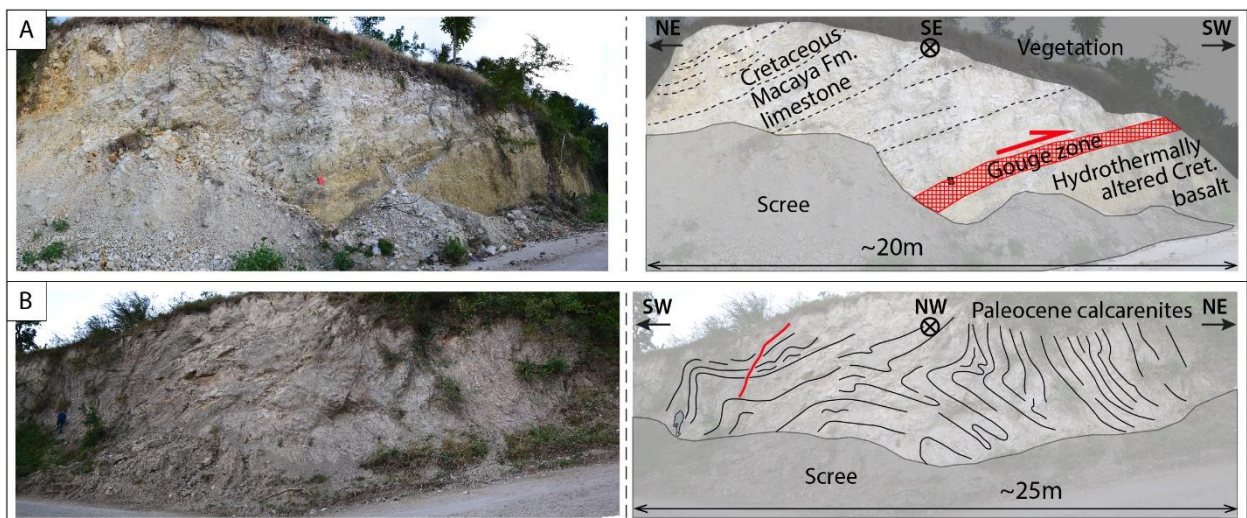


**Fig. 7a:** Thrust contact between Macaya Formation limestones and CLIP basalts. Contact is brecciated and underlying basalts are hydrothermally altered. Location on Fig. 11; SE of Mornes. **Fig. 7b:** Tight southwest verging folds within Paleocene calcarenites. Location on Fig. 11; SE of Mornes.

#### 4.3.3 Massif de la Selle

On the southern flank of the La Selle anticline, northeast of Marigot (Fig. 2b), the lower Paleocene sequences are mildly folded and overlain by relatively undeformed upper Paleocene to Eocene formations. Similar observations were made by Van den Berghe (1983), who proposed a minor unconformity between the lower and upper Paleocene formations.

West of Obleon (Fig. 2b), on the northern flank of the Massif de la Selle, a 30° NNE dipping fault with unknown sense separates Cretaceous basalts from Eocene platform limestones (Fig. 8a).

The core of the EPGFZ south of Port-a-Prince (Fig. 2b) consists of a more than 200m wide zone of re-cemented limestone breccia (Fig. 8b). This is comparable to the 500m wide zone of disrupted sediments representing the core of the EPGFZ in Lake Miragoane and Lake Azuei (Wang et al., 2018) and west of Léogâne (Hornbach et al., 2010). The tectonically pulverized rock from the fault core is used as building material and mined in quarries that are located along the EPGFZ. At the quarries of La Boule and Toto (Fig. 2b), predominantly south-dipping and east – west trending polished fault mirrors range from a few meters to 100m in size. Some of the fault surfaces are undulating along sub-vertical and sub-horizontal axes (Fig. 8b). The sense of motion on oblique faults that are in a Riedel configuration to the E – W trending fault mirrors is mainly sinistral on sub-horizontal kinematic indicators and reverse on sub-vertical ones. The sub-horizontal trends are overprinted by the sub-vertical trends.

At Boutillier quarry (Fig. 2b) large fault mirrors with undulating surfaces are dipping steeply to the north. Kinematic indicators show reverse motion with a north-side-up component.

At Les Cayettes quarry (Fig. 2b) a 45° east-dipping thrust fault separates a lower to middle Miocene hanging wall from an upper Miocene – lower Pliocene footwall (Fig. 8c). East-west trending sub-vertical faults with inclined striations are only observed in the hanging wall and not in the footwall. These striations dip 45° to the east, similar to the orientation and dip of the thrust. This indicates that the vertical strike-slip faults are older and displaced by the thrust.

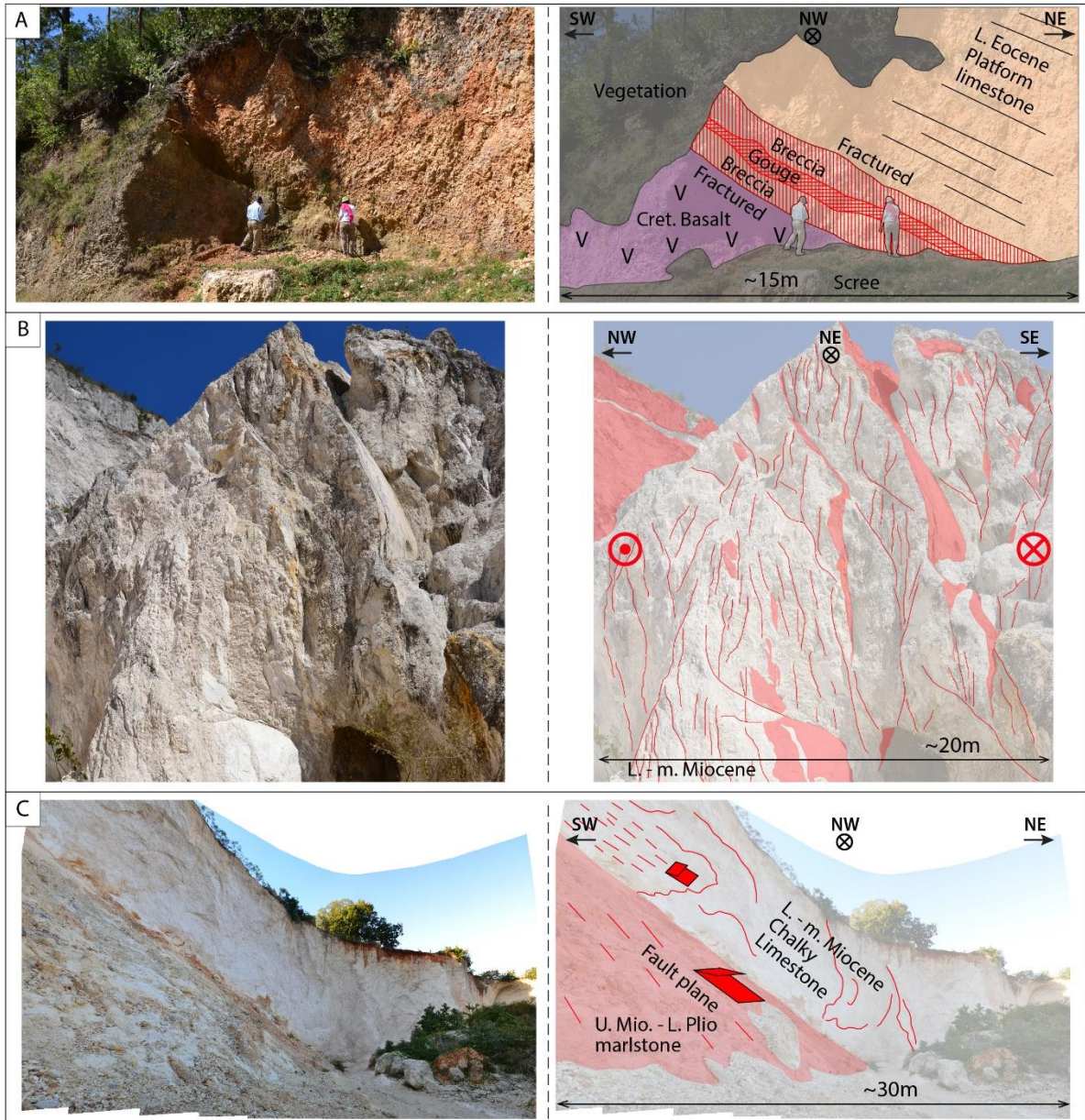


**Fig. 8a:** Fault with unknown sense of motion separating Eocene platform limestones from CLIP basalts. Location on Fig. 13; west of Obleon, northern flank of Massif de la Selle. **Fig. 8b:** Fault core of the EPGFZ. South-dipping, east – west trending fault mirrors. Location on Fig. 13; La Boule quarry. **Fig. 8c:** Southwest verging thrust separating upper Miocene – lower Pliocene marlstones in the footwall from lower to middle Miocene chalky limestones in the hanging wall. Location on Fig. 13; Les Cayettes quarry.

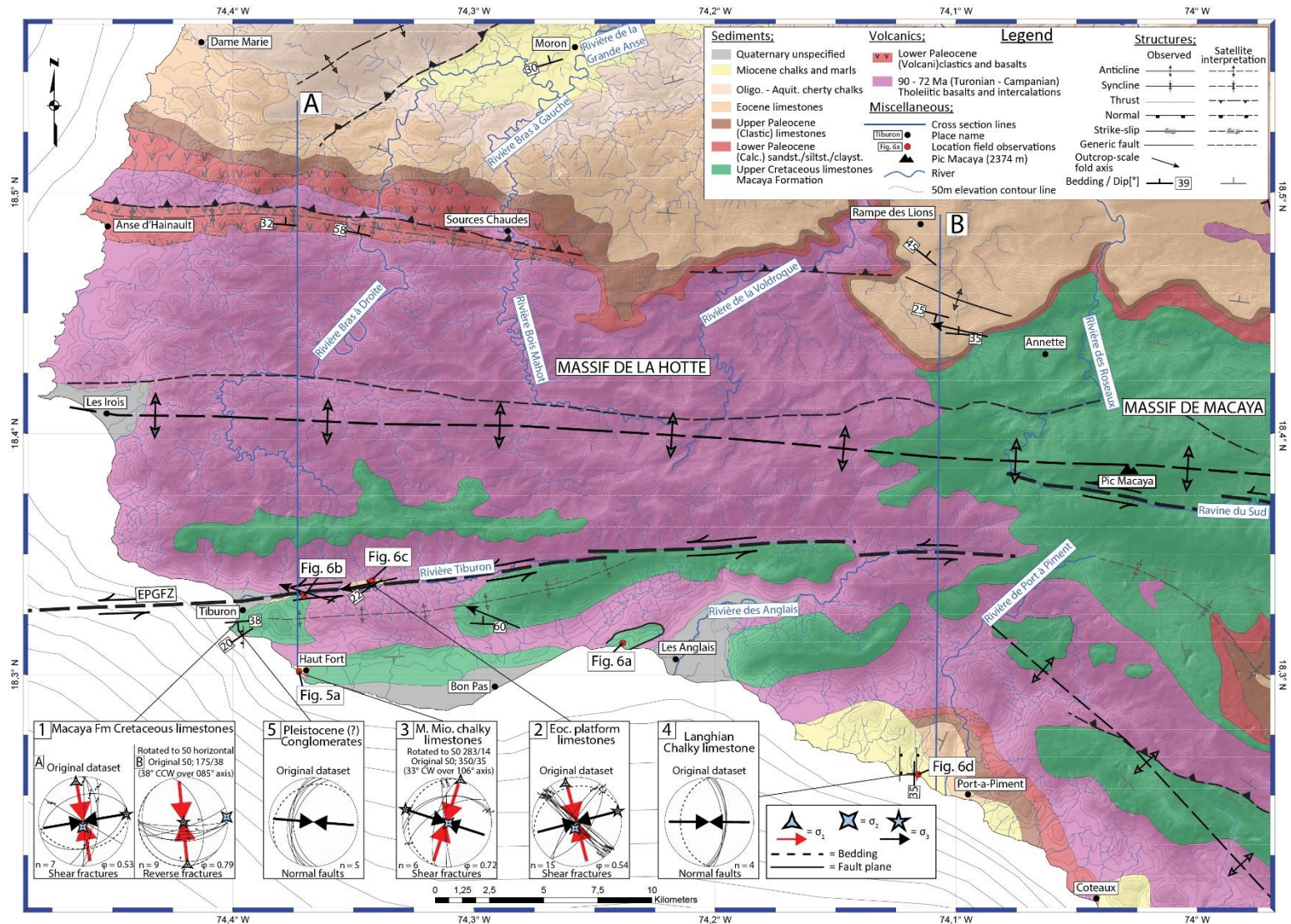
#### **4.4 Map-scale deformation structures**

##### 4.4.1 Western Massif de la Hotte

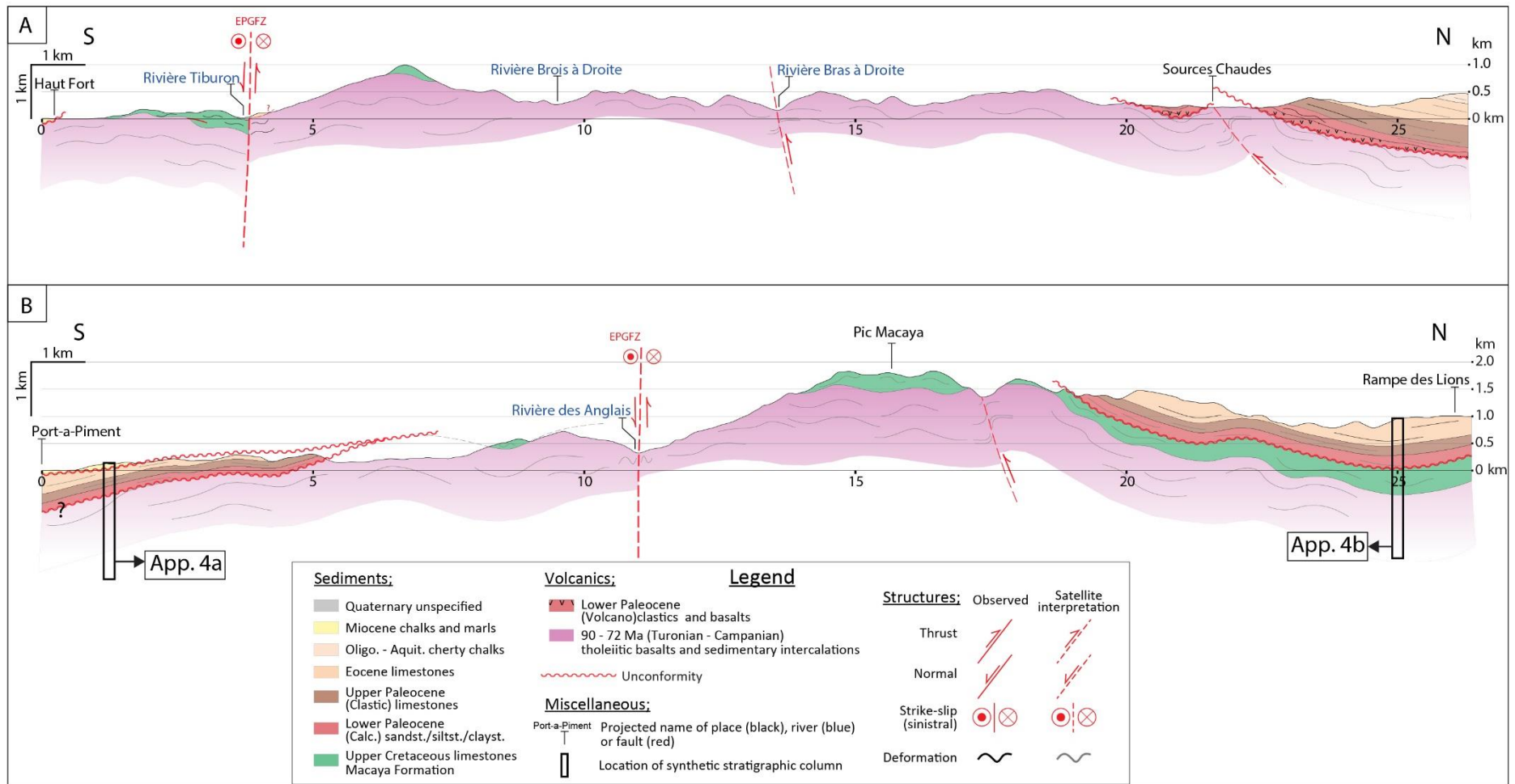
The largest first-order fold is an E – W trending 10 km half-wavelength anticline that continues from Les Irois in the west through the Macaya Massif in the east (Fig. 9). This fold is tighter in the east (Fig. 10b) than in the west (Fig. 10a). In the map area where the sedimentary cover is lacking (Fig. 10), it is difficult to observe any structuration within the Cretaceous basalts on satellite imagery. The second order folding shown on cross section A (Fig. 10a), with wavelengths of around 5 kilometers, is interpretative and based on the topography, folding observed on the onshore cross section B (Fig. 10b) and on offshore seismic profiles (for instance line CT2-28 from Mann et al. (1995)).

The E – W trending topographic lineament that is expressed in the morphology east of Tiburon is considered to be the trace of the EPGFZ (Fig. 9; Mann et al., 1984). This lineament consists of at least five segments in the mapped area. Close to Tiburon the valley widens and the morphological expression of the EPGFZ becomes less pronounced. In map view we cannot identify any clear lateral offset of lithological units. Based on the difference in elevation of the Macaya limestones on both sides of the Tiburon Valley (Fig. 10a) a vertical offset is inferred and estimated at around 1000m. Another east – west trending topographic lineament, although less prominently expressed in the morphology compared to the EPGFZ, originates at Les Irois, continues east for around 40 kilometers, and is displacing the course of the Rivière Bras à Droite and Rivière Bois Mahot (Fig. 9). Further east this trace undulates and it is unclear if a single fault is still present north of the Pic Macaya. These lineaments are interpreted as the surface traces of strike-slip faults. Based on field observations, the deformation accommodated on each of them appears however scarce.





1 **Fig. 9:** Geological map of the Tiburon area. For location see **Fig. 2b**. Black bedding symbols with dip in degrees are measured in the field.  
 2 Black fold axes represent folds constructed using outcrop measurements. Bedding symbols in grey are obtained using satellite imagery. Solid black lines are observed structures, dashed black lines denote  
 3 structures from literature, while dashed grey lines are structures based on satellite image interpretation.



4 **Fig. 10:** One-to-one scale cross sections of the western Massif de la Hotte. Locations of cross sections in Fig. 9. The topography is derived using ASTER DEM data. Faults  
 5 shown as solid red lines are observed while dashed red lines are from satellite interpretation. Grey lines within the formations denote the inferred general trend of the  
 6 bedding, which schematically shows tighter folding in the Cretaceous formations compared to the Cenozoic formations. Only the large-scale structures are shown. Dip of  
 7 EPGFZ unknown. Abbreviations; App. = Appendix, EPGFZ = Enriquillo – Plantain Garden Fault Zone.



Between Anse-d'Hainault and Source Chaudes an E – W trending, south-verging thrust is inferred based on the mapping by Calmus (1983) and Amilcar (1997) and the measured dip of the lower Paleocene to the south of the fault (Fig. 9). This fault, if mapped correctly, runs through the area of hot springs at Sources Chaudes, displaces lower Paleocene clastics and Cretaceous basalts (Calmus, 1983), but based on satellite images does not displace the upper Paleocene or younger lithologies. This indicates that this thrust fault is of pre- late Paleocene age (Fig. 10).

#### 4.4.2 L'Asile region

The EPGFZ in the mapped area (Fig. 11) consists of a continuous northern segment and a shorter southern segment, both of which are acting as boundaries to the Clonard Basin. The EPGFZ offsets mapped lithological units north and south of its trace. A change in vertical motion occurs along the trace of the EPGFZ in this area, with the l'Asile Basin (section C, Fig. 12c) displaying south-side up and the Clonard Basin (section A, Fig. 12a) displaying north-side up motion. The Clonard Basin is trending E – W and is bounded by faults to the north and south, which continue as far west as Camp Perrin (Mann et al., 1983, 1995). Neither on satellite data nor in the field could we identify a fault acting as the northern boundary to the WNW-trending l'Asile Basin, which appears only bounded to the south by the EPGFZ (Fig. 11).

Several second-order WNW – ESE trending synclines and anticlines with wavelengths in the order of 5 km were observed on satellite images in the region north of the EPGFZ (Fig. 11 and Fig. 12). The wavelengths of these structures are comparable to the wavelengths of fault-controlled folds observed on seismic data offshore between the Southern Peninsula and Gonâve Island (Bien-Aime Momplaisir, 1986; Mann et al., 1995). We have no field or satellite image based evidence to support that the onshore folds are also fault-controlled.

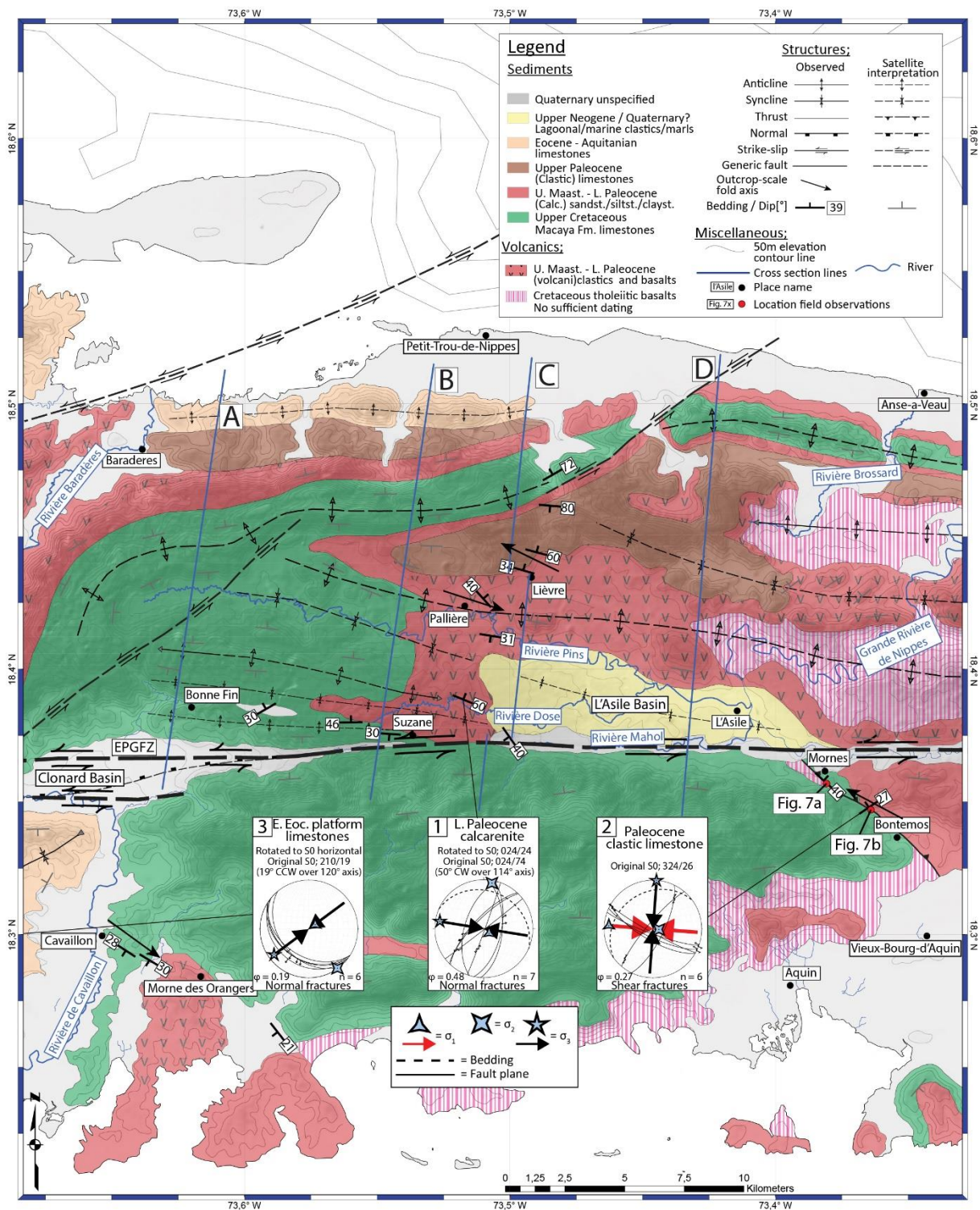
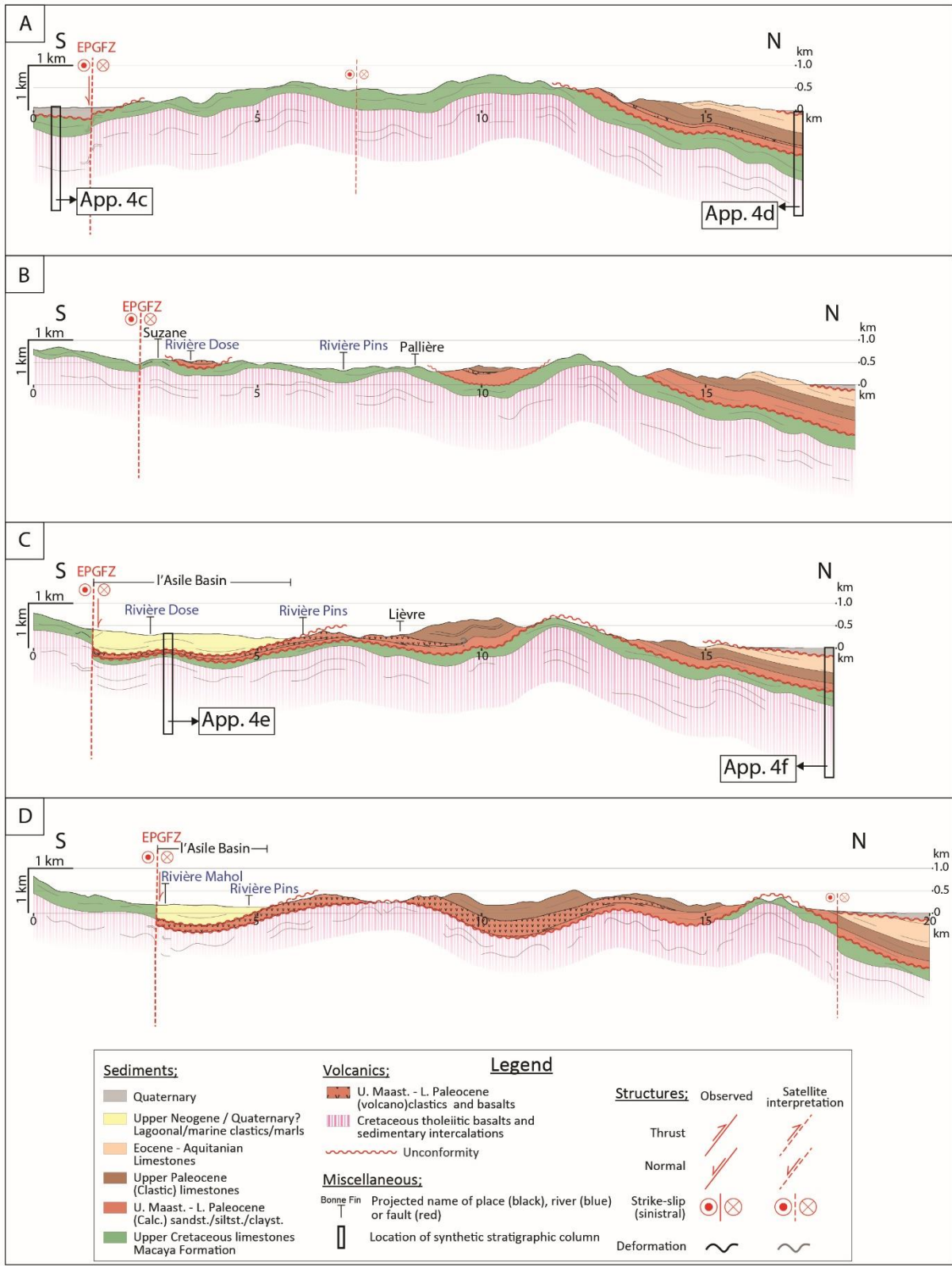


Fig. 11: Geological map of the l'Asile area. For location see Fig. 2b. Symbols are the same as described in the caption of Fig. 9.



**Fig. 12:** One-to-one scale cross sections of the l'Asile Basin area. Locations in Fig. 11. Symbols are the same as described in the caption of Fig. 10. Dip of EPGFZ unknown. Tighter folding within the Cretaceous formations compared to the Cenozoic formations schematically represented.

#### 4.4.3 Massif de la Selle

The two dominant structures on the map are the N080°E trace of the EPGFZ and the roughly E – W trending axis of the Massif de la Selle anticline (Fig. 13). This anticline has a wavelength of around 40 km and is mildly asymmetric, with a gentle southern limb and a slightly steeper northern limb. Second-order folding with a 5 km wavelength is more open compared to the other cross sections (Fig. 13 and Fig. 14). Within the Cretaceous basalts in the central part of the anticline we were unable to identify any folding based on satellite images or topography.

West of Obleon, on the northern flank of the anticline, the Paleocene is missing, with a fault marking the contact between the Eocene and the Cretaceous (Fig. 13 and Fig. 14). The sense of motion on this fault could not be determined. An upper Maastrichtian to lower Paleocene series is identified in the Beloc region on the northern flank of the anticline (Fig. 2b; ‘Jacmel Blocks’ of Mercier de Lépinay et al., 1979). This indicates that the Paleocene is deposited on the northern flank and is the reason for interpreting it in Fig. 13.

The labelled faults bordering the Cul-de-Sac plain (Fig. 13) are taken from the work of Terrier et al. (2014) and Saint Fleur et al. (2015), which are verified using satellite imagery. According to these authors and to Symithe and Calais (2016), the folds in the southern Cul-de-Sac plain are fault-propagation folds bounded by predominantly south-southwest dipping thrusts. Wang et al. (2018) identified the John Brown Ave thrust (J.B. Ave Fault; Fig. 13) to be northeast-dipping, which in our interpretation is a secondary, antithetic fault to the dominantly SSW dipping thrusts in this region.

The previously unnamed fault between Fermate and Kenscoff (Van den Berghe, 1983a) is labelled Redoute after the corresponding river valley, while the Chauou fault is named after the town on the crest of the anticline directly south (Fig. 13). We interpret the Redoute and Chauou faults as south-dipping thrusts, since they juxtapose an anticline of older sequences to the south against younger sequences to the north (Fig. 13 and Fig. 14). In map view the thrust faults terminate against the EPGFZ.

This indicates that these thrusts are either; 1) synchronous or post-dating the EPGFZ and are abutting against it (scenario 1, Fig. 14a), or 2) that they are older and subsequently offset by the EPGFZ (scenario 2, Fig. 14b).



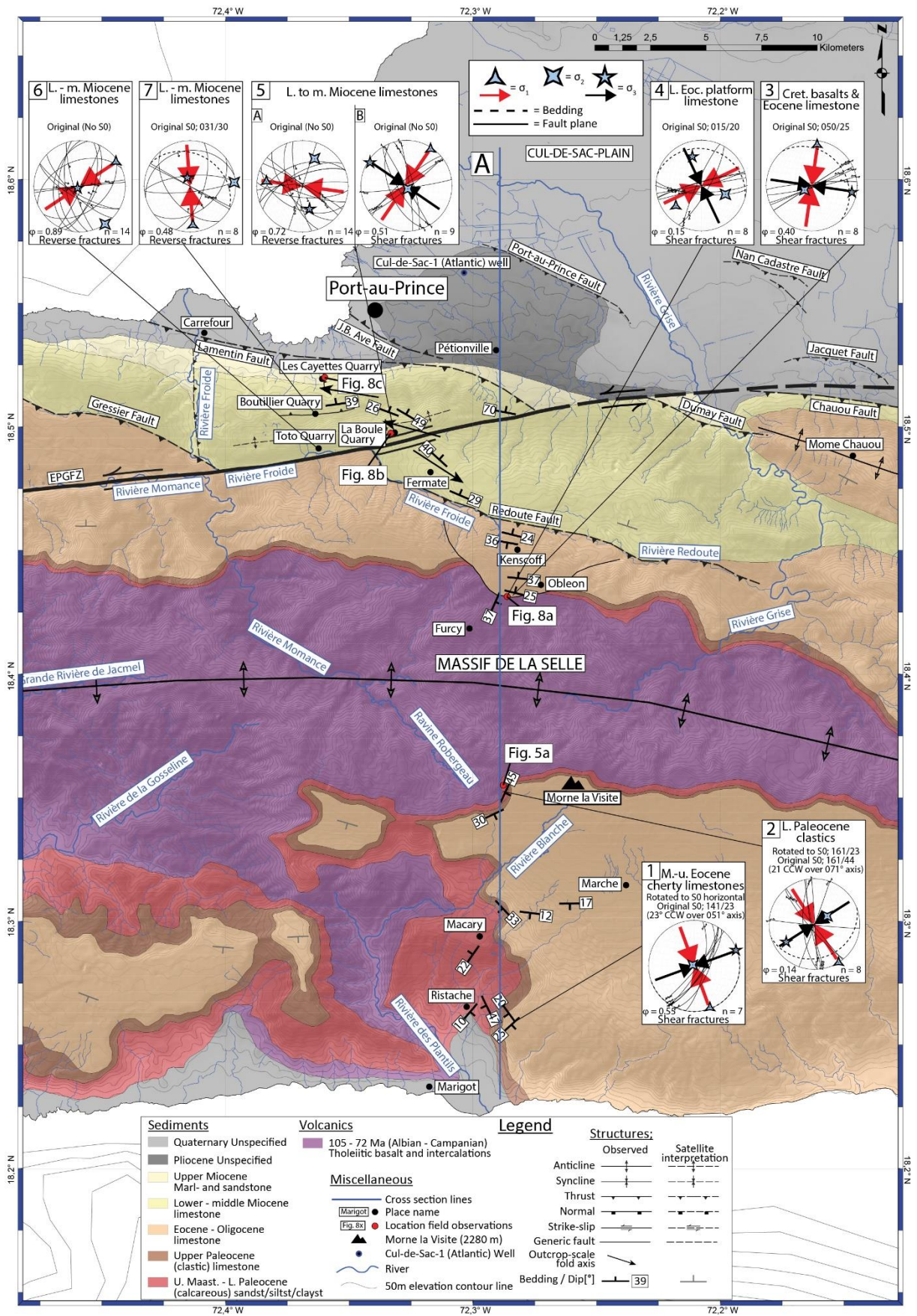
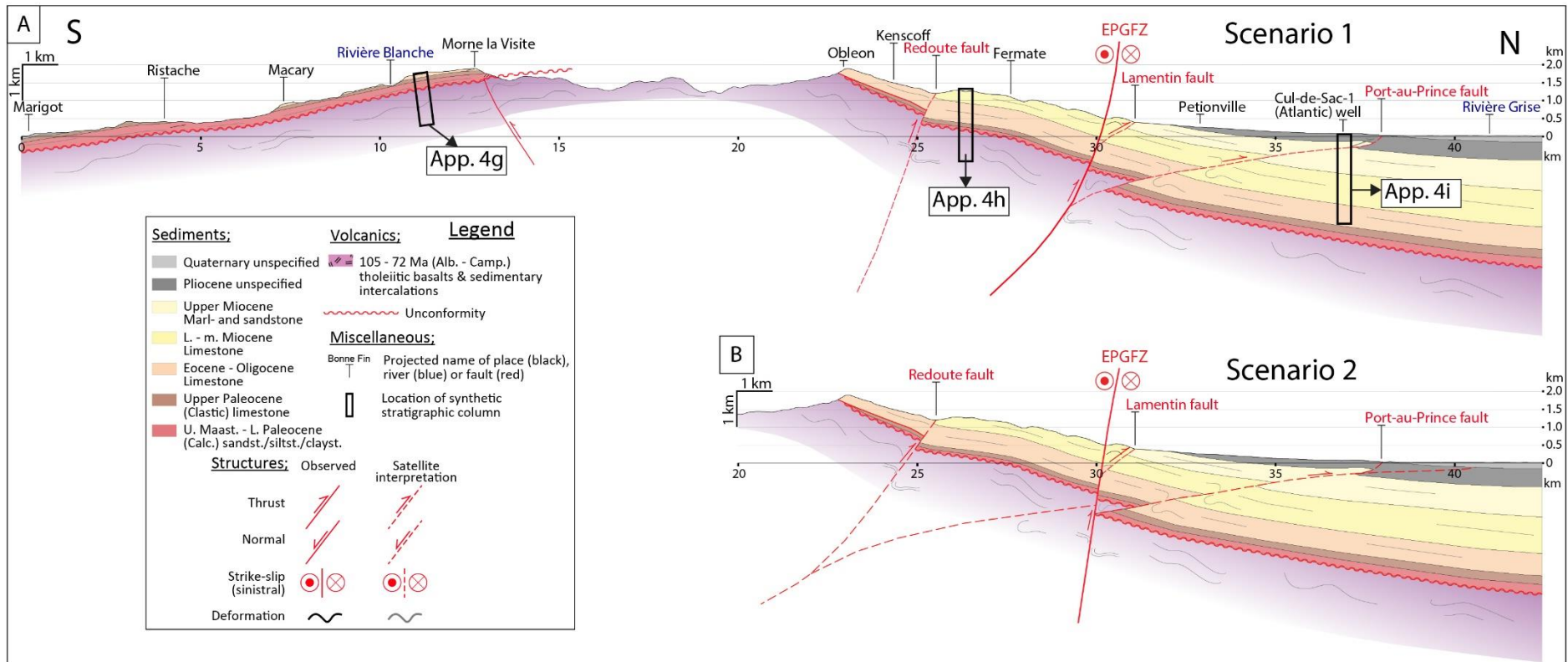


**Fig. 13:** Geological map of the Marigot area. For location see Fig. 2b. Symbols are the same as described in the caption of Fig. 9.



1 **Fig. 14:** One-to-one scale cross section of the Massif de la Selle. Locations in **Fig. 13**. Symbols are the same as described in the caption of **Fig. 10**. Tighter folding within the  
 2 Cretaceous formations compared to the Cenozoic formations schematically represented.

## **4.5 Paleo-stresses and relative timing**

### 4.5.1 Western Massif de la Hotte

Within the Macaya Formation limestones south of Tiburon (Fig. 9.1), set 1A shear fractures were formed by a strike-slip regime with NNW - SSE trending  $\sigma_1$  axis. Set 1B resulted from a reverse regime with north – south trending  $\sigma_1$  axis. In the present-day orientation set 1A is in an Andersonian configuration. Back-tilting the bedding to a horizontal position restores the set 1B strike-slip stress regime to an Andersonian configuration. This suggests that set 1B originated prior to tilting of the bedding and formed before set 1A shear fractures, and that reverse faulting preceded strike-slip.

Lower Eocene platform limestones in the Tiburon valley, proximal to the trace of the EPGFZ, have pervasive and regularly spaced orthogonal joints that are reactivated as shear fractures (Fig. 9.2). Reactivation resulted from a strike-slip regime with NNW – SSE trending  $\sigma_1$  axis, which is similar to set 1A, possibly indicating that both were created post- early Eocene. Middle Miocene chalky limestones southeast of Tiburon at Haut Fort yielded one set of shear fractures that resulted from a reverse regime with NNE – SSW trending  $\sigma_1$  axis (Fig. 9.3). Back-tilting over an E – W trending axis restores the stress regime to an Andersonian configuration, which indicates that the bedding was mildly tilted to the west before being affected by the reverse stress regime. Two sets of normal faults are observed. One set is located in the middle Miocene (Langhian?) chalky limestones northwest of Port-a-Piment (Fig. 9.4), while another set is situated in the Plio-Quaternary conglomerates south of Tiburon (Fig. 9.5). Both sets indicate E – W oriented extension.

The above results can be summarized as follows: (1) reverse regime with N – S  $\sigma_1$  axis between post-Maastrichtian and probably pre-Eocene times, followed by (2) strike-slip regime with NNW – SSE  $\sigma_1$  axis in post- early Eocene times, (3) reverse regime with NNE – SSW  $\sigma_1$  axis during post- early Miocene times, and (4) post- Langhian through Plio-Quaternary extensional regime with E – W  $\sigma_3$  axis. No relative timing could be established between the last three deformation phases.

#### 4.5.2 L'Asile region

Conjugate shear fractures with variably plunging striations were found in the steeply dipping calcareous beds of the lower Paleocene volcanoclastic sequence along the Rivière Dose (Fig. 11.1). Back-tilting this dataset resulted in an Andersonian extensional stress regime with E – W trending  $\sigma_3$  axis.

Paleocene clastic limestones between Mornes and Bontemos (Fig. 11.2) contain shear fractures with sub-horizontal striations. Stress inversion on these fractures in their present-day orientation results in an Andersonian strike-slip regime with east – west trending  $\sigma_1$  axis. NW – SE trending normal faults were found in lower Eocene limestones west of Cavillon (Fig. 11.3). Stress inversion and subsequent back-tilting of the data results in a NE – SW trending  $\sigma_3$  axis.

No cross-cutting relations could be established between the different fault sets, with the relative timing based on the ages of the lithologies summarized as follows: (i) post- early Paleocene extensional regime with E – W trending  $\sigma_3$  axis, (ii) post- Eocene extensional regime with NE – SW trending  $\sigma_3$  axis, and (iii) post- Paleocene strike-slip regime with E – W trending  $\sigma_1$  axis. Although there is no relative timing of deformation, the strike-slip regime (Fig. 11.2) is probably a young deformation event, since it took place when the bedding was already roughly in its present-day orientation.

#### 4.5.3 Massif de la Selle

Lower Eocene limestones east of Ristache have NE – SW trending left-lateral shear fractures resulting from a back-tilted strike-slip regime with NNW – SSE trending  $\sigma_1$  axis (Fig. 13.1). Lower Paleocene sediments west of Morne La Visite are fractured by a back-tilted strike-slip regime with NNW – SSE trending  $\sigma_1$  axis (Fig. 13.2). Both these stress regimes are similar, suggesting that they initiated post-early Eocene.

On the northern flank, in both the Cretaceous basalts and Eocene limestones directly adjacent to the faulted contact west of Obleon, left-lateral shear fractures resulted from a strike-slip regime with NNE – SSW trending  $\sigma_1$  axis (Fig. 13.3). At this locality it is unclear if the strike-slip regime pre- or post-dates the faulted contact. A strike-slip regime with NE – SW trending  $\sigma_1$  axis fractured Eocene limestones directly west (Fig. 13.4). It is not possible to back-tilt this dataset to an Andersonian configuration using only the bedding, possibly indicating a local variation in the stress regime.

In the core of the EPGFZ at La Boule quarry we identified distinct sets of shear fractures, whose inversion points to two distinct paleo stress states (Fig. 13.5). Because the measurements were taken within the core of the fault the obtained stresses may reflect the local rather than the far field stress state. Set 5A and 5B have an E – W and NE – SW trending  $\sigma_1$  axis, respectively. Reverse striations that dominate set 5A overprint strike-slip striations of set 5B, indicating that reverse faulting is younger than strike-slip at this location. The NE – SW orientation of the  $\sigma_1$  axis at Toto Quarry (Fig. 13.6) is similar to set 5B at La Boule, and both measurement sites are located in the core of the EPGFZ. The difference is that stress state 6 at Toto is reverse, while 5B at La Boule is strike-slip. At Boutillier quarry thrusting resulted from a reverse regime with N – S trending  $\sigma_1$  axis (Fig. 13.7). At Les Cayettes quarry, striations on strike-slip faults, which are only observed in the lower to middle Miocene hanging wall (Fig. 8c), have a similar plunge as the dip of the thrust fault. This suggests that the strike-slip faults are older than the thrust and were subsequently transported onto the upper Miocene – lower Pliocene footwall. This indicates that strike-slip activity occurred roughly pre- latest Miocene, with thrusting roughly post- earliest Pliocene.

The above results can be summarized as follows for the Massif de la Selle. Southern flank: Post- early Eocene strike-slip regime with NNW – SSE trending  $\sigma_1$  axis. Northern flank: Reverse stress regimes with variably oriented  $\sigma_1$  axes are generally post-dating strike-slip stress regimes with NE – SW and NNE – SSW trending  $\sigma_1$  axes. At Boutillier quarry the timing is constrained to (1) Pre- late Miocene strike-slip and (2) post- earliest Pliocene thrusting.



#### 4.6 Compilation of kinematic data

Stress inversion of kinematic fault slip data obtained at 22 sites resulted in a total of 26 reduced stress tensors. The spatial distribution of paleostresses along the EPGFZ are plotted on the map in Fig. 15a.

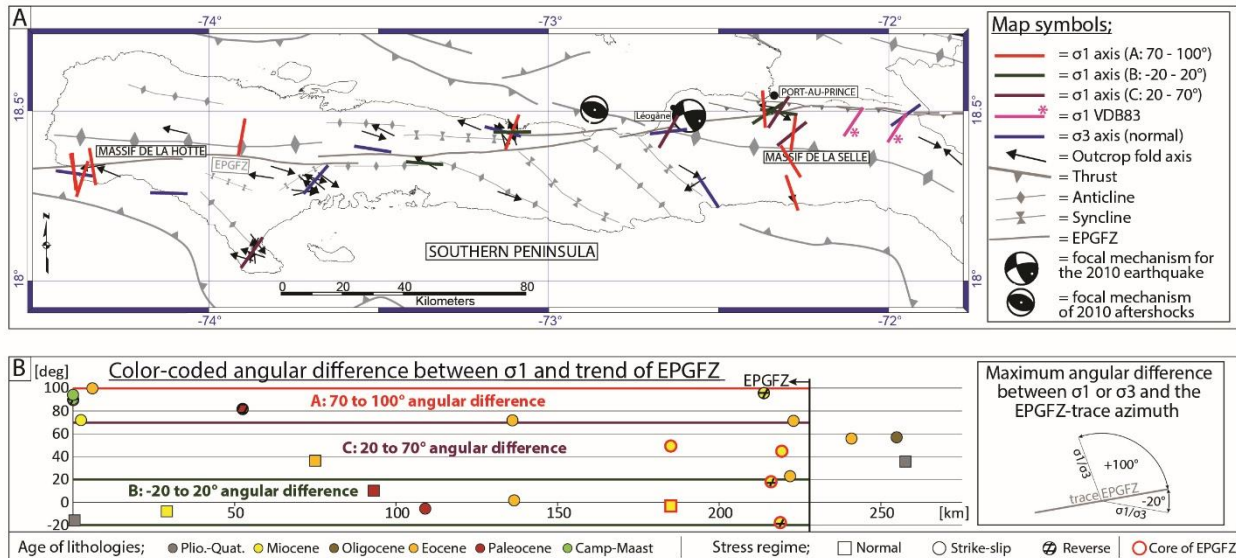


**Fig. 15a:** Plot of trends of sigma 1 (black) and sigma 3 (blue) axes from stress inversion results. Fold axes derived from outcrops are plotted in green. **Fig. 15b:** Chart showing angular difference (degrees) between trend of the sigma 1 or sigma 3 axes and the trace of the EPGFZ. Colors indicate age of lithologies from which the data was obtained. Square indicates normal stress regime, circle indicates strike-slip stress regime and hashed circle indicates reverse stress regime. Results on the right-hand side are constructed using the N095°E average trend of thrusts in this region. Red circle is data from the core of the EPGFZ. Plotted results are at less than 15km distance from the EPGFZ trace. Angular difference varies between -20 and +100 degrees (see inset on right).

##### 4.6.1 Along-strike variation of stress tensors

The maximum principal stress axes can be separated into three groups (Fig. 15b). The first group has an angle with the EPGFZ varying between 70 and 100°. The second group has an angle between -20° and 20° to the EPGFZ. The third group has an angle of approximately 45° to the EPGFZ. An angle of 45° or less is obtained from data collected in the brecciated fault core of the EPGFZ. West of Léogâne a reverse regime is only found in Cretaceous and lower Paleocene formations. East of Léogâne reverse regimes are found in lower to middle Miocene limestones.

The minimum principal stress axes for normal regimes are either at around 45° to strike of the EPGFZ or grouped between -20° to 10°, hence sub-parallel to the EPGFZ.

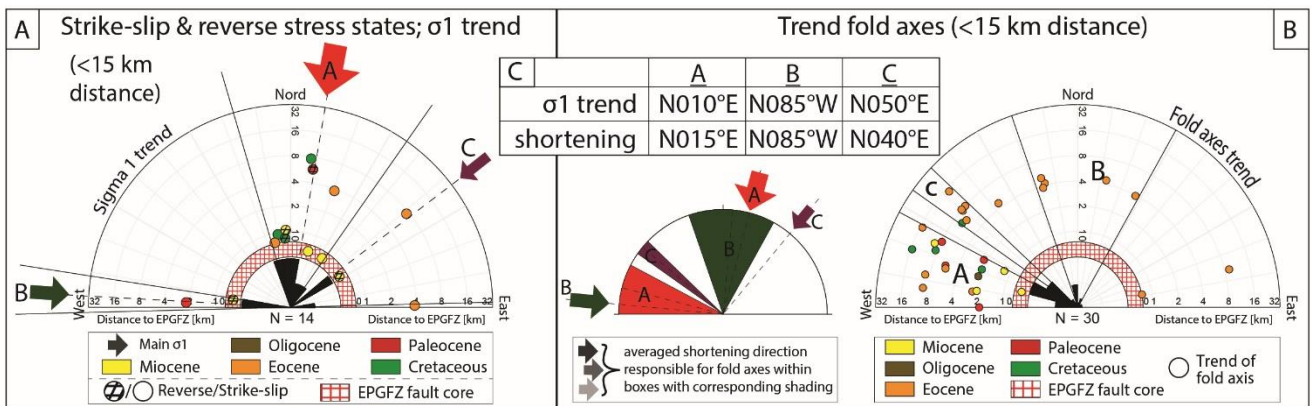


**Fig. 16a:** Plot showing trend of sigma 1 axes vs distance to the trace of the EPGFZ for measurements within 15 km of this fault. Arrows indicate dominant trends. Measurements obtained from the fault core are within the red hashed zone. **Fig. 16b:** Same principle as figure 16a but for fold axes derived from outcrops. **Fig. 16c:** Comparison between groups A, B and C from averaged  $\sigma_1$  trend and averaged axes of contraction.

#### 4.6.2 Direction of maximum principal stress versus maximum shortening

The trend of the maximum principal stress axes versus the distance to the trace of the EPGFZ is plotted in Fig. 16a and can be subdivided into three groups. The dominant group A has an averaged N010°E trend for the axis of maximum principal stress (Fig. 16c). Two minor groups of data, B and C, have an averaged trend of N085°W and N050°E for the axis of maximum principal stress, respectively (Fig. 16c). For a distance less than 15 km from the EPGFZ, there is no apparent correlation between distance to the fault and paleostress orientation (Fig. 16a).

The trends of the fold axes constructed using bedding measurements is shown in Fig. 16b. Care has been taken in the field to distinguish gravity-related slumps, which are frequently occurring in well-bedded cherty limestones of Cretaceous and Eocene – early Miocene age, from tectonically-related folds. The first-order dominant fold axes trend WNW, which can be subdivided into group A (N075°W) and group C (N050°W) based on the arguments presented in section 5.4. A minority of fold axes is scattered around N005°E in group B. The corresponding direction of maximum contraction for these fold axes is N015°E (group A), N085°W (group B) and N040°E (group C) (Fig. 16c).

From Fig. 16c it is noticeable that for groups A, B and C, the orientation of the maximum principal stress axes is sub-parallel to the axes of maximum contraction. Apart from two paleostress data points from the core of the EPGFZ, both the fold axes and paleostress states for the three groups affect the same lithologies (Fig. 16a and Fig. 16b).

## 5. Discussion

### ***5.1 Maastrichtian – early Paleocene deformation phase; local folding, thrusting, and erosion***

The existence, extent, and structural implications of a Late Cretaceous to Paleocene tectonic event on the Southern Peninsula are subject to debate, with authors arguing in favor (Mercier de Lépinay et al., 1979; Calmus, 1983; Van den Berghe, 1983a; Bien-Aime Momplaisir, 1986; Calmus and Vila, 1988) or against (Maurrasse, 1982; Desreumaux, 1985b; Bourgueil et al., 1988; Amilcar, 1997) such a deformation phase.

The first two arguments of the authors in favor of this deformation phase focus on the stratigraphic unconformity between the Cretaceous and Paleogene formations and the presence of Cretaceous erosional products within the lower Paleocene formations. The compilation map of Cretaceous and Paleocene biostratigraphic data (Fig. 4a) clearly shows the presence of a Maastrichtian to early Paleocene unconformity. Erosion was strongest in the Anse-d'Hainault area, along an E – W line from Port-a-Piment to Morne Orangers, and in the central Massif de la Selle region. The area around Platon Besace is not affected by this deformation, while north of Camp Perrin and south of Baraderes erosion only removed part of the Cretaceous sedimentary cover. The upper Maastrichtian to Danian clastic sequence overlying the unconformity often starts with a basal conglomerate containing clasts of Cretaceous basalts and Macaya Formation limestones (Mercier de Lépinay et al., 1979; Calmus, 1983; Van den Berghe, 1983a; Bien-Aime Momplaisir, 1986; Calmus and Vila, 1988).

The other arguments focus on a difference in deformation style and intensity between Cretaceous to lower Paleocene formations on the one hand, and the upper Paleocene and more recent formations on the other. The tightness of folds may also depend on the mechanical behavior of the lithology to compression, which is influenced by layer thickness and the type of lithology. There are however no first-order lithological differences between the Cretaceous Macaya Formation and the middle Eocene to early Miocene formations. Both consist of dm-bedded chalky limestones with cherts. The early

Eocene limestones have a similar bed thickness, but consist of platform facies without cherts (Calmus, 1983; Van den Berghe, 1983a; Desreumaux, 1985b; Bourgueil et al., 1988).

The Cretaceous limestones in the Tiburon Valley are tightly folded around WNW-trending axes, while lower Eocene limestones in this valley are only mildly folded and deformed around ENE-trending axes (Fig. 6b and Fig. 6c). Any deformation resulting from activity on the EPGFZ, which runs through this valley as well, can be expected to have a similar effect on both lithologies. The difference in style and intensity of deformation is thus not related to activity on the EPGFZ. It is probable that this difference in style results from a deformation event occurring prior to deposition of the lower Eocene limestones, and post-dating deposition of the Macaya Formation limestones. The most likely candidate is the Cretaceous to early Paleocene deformation that is also responsible for the associated unconformity.

Calmus (1983) and Calmus and Vila (1988) also described a difference in the style and intensity of deformation between Cretaceous to lower Paleocene, and upper Paleocene to younger formations. These authors observed a NE-vergence for structures within the Cretaceous and early Paleocene formations. Our own field observations contradict this, with most structures displaying a vergence towards the south or southwest (Fig. 9a and Fig. 9b), with a minority showing top-to-north or northeast motion (Fig. 8c).

Calmus (1983) and Calmus and Vila (1988) also proposed that the Macaya Formation was transported as a thin-skinned thrust sheet over the Cretaceous basalts towards the NE, over distances up to 30 km. We observed that in large parts of the Southern Peninsula the Macaya Formation is not eroded, only mildly deformed and in a stratigraphic contact with the underlying Cretaceous basalts. We found no evidence supporting the transport of the Macaya Formation as a thrust sheet over the Cretaceous basalts and the lower Paleocene units. Deformation and uplift probably resulted from a crustal-scale buckling-style of folding (Fig. 10 and Fig. 12), which can explain the lateral differences in the amount of erosion of the Cretaceous formations.



## ***5.2 Early Miocene deformation phase; local folding, minor thrusting, and erosion***

The existence of this deformation phase strongly hinges on the existence of early Miocene erosional unconformities. Our compilation map of biostratigraphic data (Fig. 4b) shows an E – W trend in the amount of erosion of Aquitanian and older units, which is decreasing eastwards. Around 1000m of erosion occurred in the southwestern Massif de la Hotte, while sedimentation was continuous throughout most of the Massif de la Selle. This compilation also shows a general correlation between the amount of erosion and the onset of post-erosion sedimentation; the stronger the erosion, the younger the age of the overlying units. The timing of deformation responsible for this erosion is probably Aquitanian in age, as indicated by the intra-Aquitanian unconformity at Platon Besace (Fig. 4b). The paleo-topography created by the uplift in the western Southern Peninsula only became submerged during middle Miocene times.

Calmus (1983) and Bizon et al. (1985) have related this early Miocene phase of uplift to strike-slip activity along the EPGFZ, because they noted that some of the unconformities occur proximal to the trace of the EPGFZ. Although the unconformities trend along-strike of the EPGFZ (Fig. 4b), we doubt that strike-slip activity on the EPGFZ caused early Miocene uplift and erosion. Firstly, erosion gradually decreases eastwards and the effects of erosion are known to affect the area up to at least 15 km distance to the trace of the EPGFZ, for instance at Port-a-Piment (Fig. 4b). This contrasts with offshore observations along the active trace of the EPGFZ between Haiti and Jamaica (Leroy et al., 2015; Corbeau et al., 2016b; a), where transpressional and transtensional structures are irregularly distributed along, but always within a few kilometers distance to, the trace of the EPGFZ. The observed pattern for the early Miocene unconformity onshore (Fig. 4b) better matches with large-wavelength folding as shown on the cross sections (Fig. 10 and Fig. 12). Secondly, the middle to early late Miocene is characterized by homogeneous marine sedimentation without evidence for tectonic activity. Early Miocene activity on the EPGFZ should thus have ceased during the middle Miocene, only to become active again in the late Miocene. There is no evidence to support such behavior for the EPGFZ.

### ***5.3 Late Miocene – present-day; strike-slip to transpressive deformation and island-wide uplift***

The most recent phase of uplift of the Southern Peninsula is recorded by a change in sedimentary facies from pelagic marls and limestones that dominated the Miocene to detrital sedimentation of marls, clays and calcareous sandstones from the latest Messinian onwards (Bourgueil et al., 1988). Labradorite found as the detrital fraction records erosion from the Cretaceous basalts (Desreumaux, (1987) in, Bourgueil et al., 1988). This indicates that during the latest Messinian, exhumation already reached the structural levels of the Cretaceous basalts in the core of the Massif de la Selle. Late Miocene uplift and deformation is also recorded in the eastern Enriquillo Valley in the Dominican Republic (Mann et al., 1991b; McLaughlin and Sen Gupta, 1991; Díaz de Neira, 2002).

Present-day compression in the Southern Peninsula is shown by GPS velocity modeling (Benford et al., 2012a; Calais et al., 2016). Using the modelled GPS velocity vectors from Calais et al. (2016) and the trend of the EPGFZ, we can derive the fault parallel and fault perpendicular GPS velocities (Fig. 2a). In the western Massif de la Hotte shortening is partitioned via 8.8 mm yr<sup>-1</sup> of EPGFZ-parallel and 4.8 mm yr<sup>-1</sup> of fault-perpendicular motion. In the l'Asile region shortening is partitioned via 8.7 mm yr<sup>-1</sup> EPGFZ-parallel and 6.0 mm yr<sup>-1</sup> perpendicular motion, while in the eastern Port-au-Prince region shortening is partitioned via 8.6 mm yr<sup>-1</sup> EPGFZ-parallel and 7.7 mm yr<sup>-1</sup> EPGFZ-perpendicular motion (Calais et al., 2016). This indicates that the EPGFZ parallel velocity is relatively constant over the Southern Peninsula, but that EPGFZ perpendicular velocities increases from west to east by around 40%.

Present-day shortening between the Massif de la Selle and the Cul-de-Sac plain is partitioned over the EPGFZ and the thrust faults bordering the Cul-de-Sac plain in the south. The EPGFZ is presently active (Mann et al., 1983, 1995; Prentice et al., 2010) and rooted in the upper mantle (Benford et al., 2012b). Activity on the thrust faults is documented by active folding of Quaternary alluvium along the Lamentin thrust (Saint-Fleur et al., 2015) and reverse faulting in Quaternary alluvium at the Dumay thrust along the Rivière Grise (Terrier et al., 2014; Saint-Fleur et al., 2015). Based on our geological map (Fig. 13)

and cross section (Fig. 14) we propose two possible scenarios for interpreting the geometry of these faults at depth (Fig. 17).

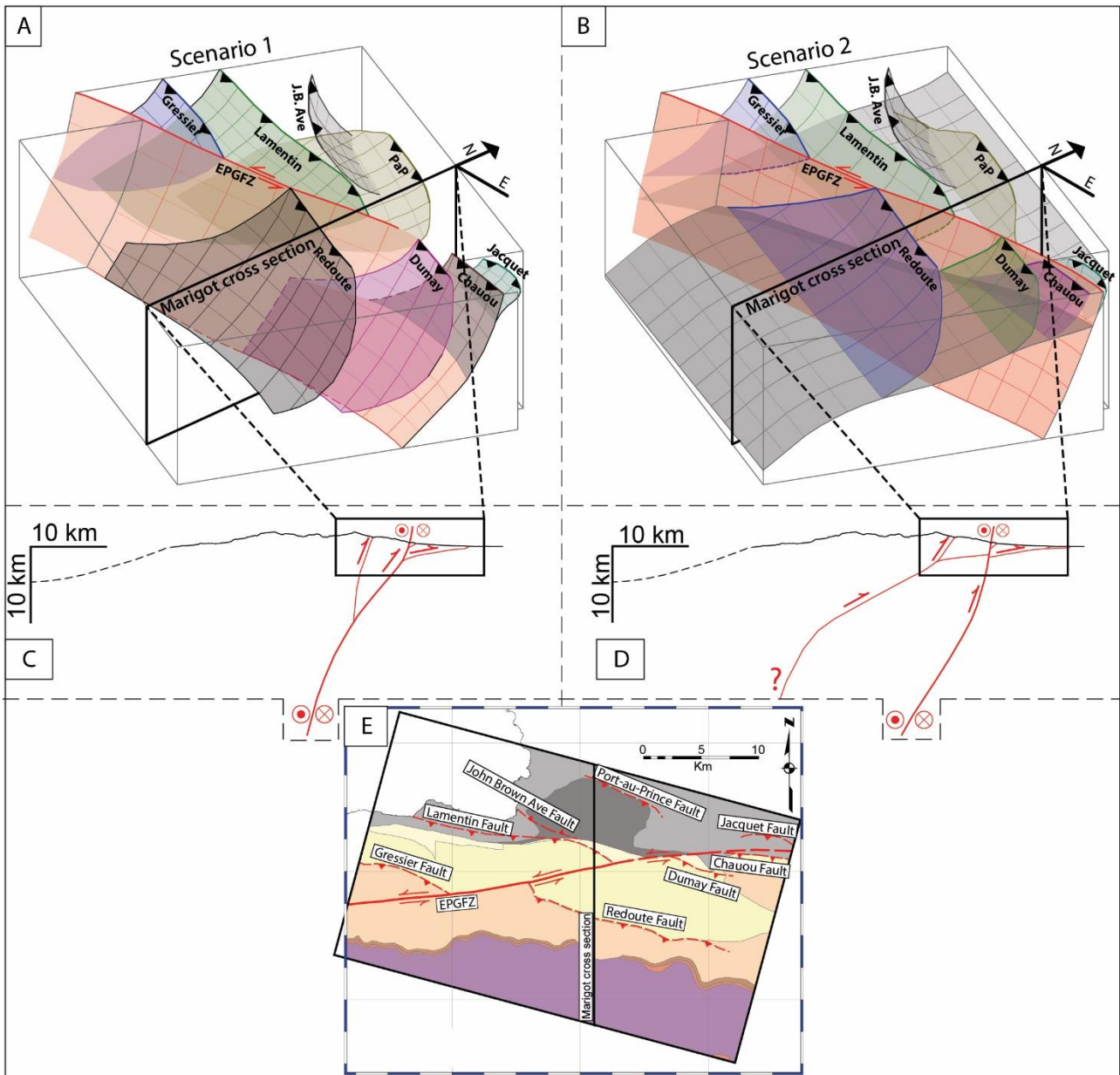


**Fig. 17:** Block cartoons showing the fault geometries corresponding to the different scenarios for the faults bordering the southern Cul-de-Sac plain. **Fig. 17a** and **Fig. 17b** correspond to scenario 1 as shown in **Fig. 14a**. **Fig. 17c** and **Fig. 17d** correspond to scenario 2 as shown in **Fig. 14b**. **Fig. 17e** is a simplified geological map from **Fig. 13**. Black box corresponds to the geographical extent of the block cartoons in Figs. 17a and 17c.

In the first scenario (#1; Fig. 17a and Fig. 17c), the Gressier and Redoute, and Lamentin and Dumay faults are not linked with each other, and all the faults are rooted on the EPGFZ. The faults to the north

have a shallow dip, whereas the faults on the southern side require a steeper dip in order to connect with the EPGFZ. The Dumay, Chauou and Jacquet faults are splay-faults rooted on the EPGFZ at depth. This scenario (#1) also explains the observation that the thrust faults on the northern side (Fig. 2a and Fig. 17e) either abut against the EPGFZ or are left-stepping and geographically proximal to the EPGFZ. We note that this scenario (#1) is essentially the same as described by Saint-Fleur et al. (2015) and modelled by Symithe and Calais (2016). The main difference is that in our conceptual model the EPGFZ is bending as it approaches the Cul-de-Sac plain and remains active as an oblique fault at depth. Another possible scenario is that the thrust faults are older and offset by the EPGFZ (#2; Fig. 17b and Fig. 17d), which is the scenario favored by Mann et al. (1995) and Wang et al. (2018). This scenario (#2) is in conflict with our observations showing that vertical striations with a reverse motion on fault planes are generally younger and cross-cutting horizontal lineations. This scenario (#2) does also not explain that the thrust faults are only found in the vicinity of the EPGFZ. We strongly favor scenario #1 where the EPGFZ is the dominant fault in the region with the thrust faults rooted on, and thus associated with the EPGFZ.

#### ***5.4 Timing of paleostress states and along-strike variation***

The reverse stress regimes found in Cretaceous and early Paleocene formations on the western part of the Southern Peninsula indicate north-south compression. At Tiburon the reverse regime is older than the strike-slip regime (conform section 4.5.1 and 5.1). Although the orientation of  $\sigma_1$  for the reverse and strike-slip regimes in this area is similar (Fig. 9.1), it is probable that these reverse regimes record the Maastrichtian – Paleocene deformation phase, since no reverse regime is observed in younger lithologies in this region. Thrust faults associated with this deformation phase trend E – W to NW – SE, indicating a general NNE – SSW directed compression (Fig. 18).

South of Maniche, Eocene to Oligocene limestones are folded along N130°E trending axes and are unconformably overlain by middle Miocene sediments (Calmus, 1983). These trends indicate a local

NE – SW oriented shortening prior to middle Miocene times. Fold axes with a similar trend are found in group C (Fig. 16b). This trend is only observed in lithologies that are Eocene or older, and predominantly in the western two-thirds of the Southern Peninsula. We therefore relate these folds to the early Miocene deformation phase (Fig. 18).

Data of group B has N085°W trending axis for both maximum principal stress and maximum shortening, which is sub-parallel to the trend of the EPGFZ (Fig. 16). This group is observed within 5 km distance to the EPGFZ and within Paleocene to middle Miocene formations. Although the reason for this sub-parallel trend is unknown, its proximity to the EPGFZ suggests that it is related to activity on this fault.

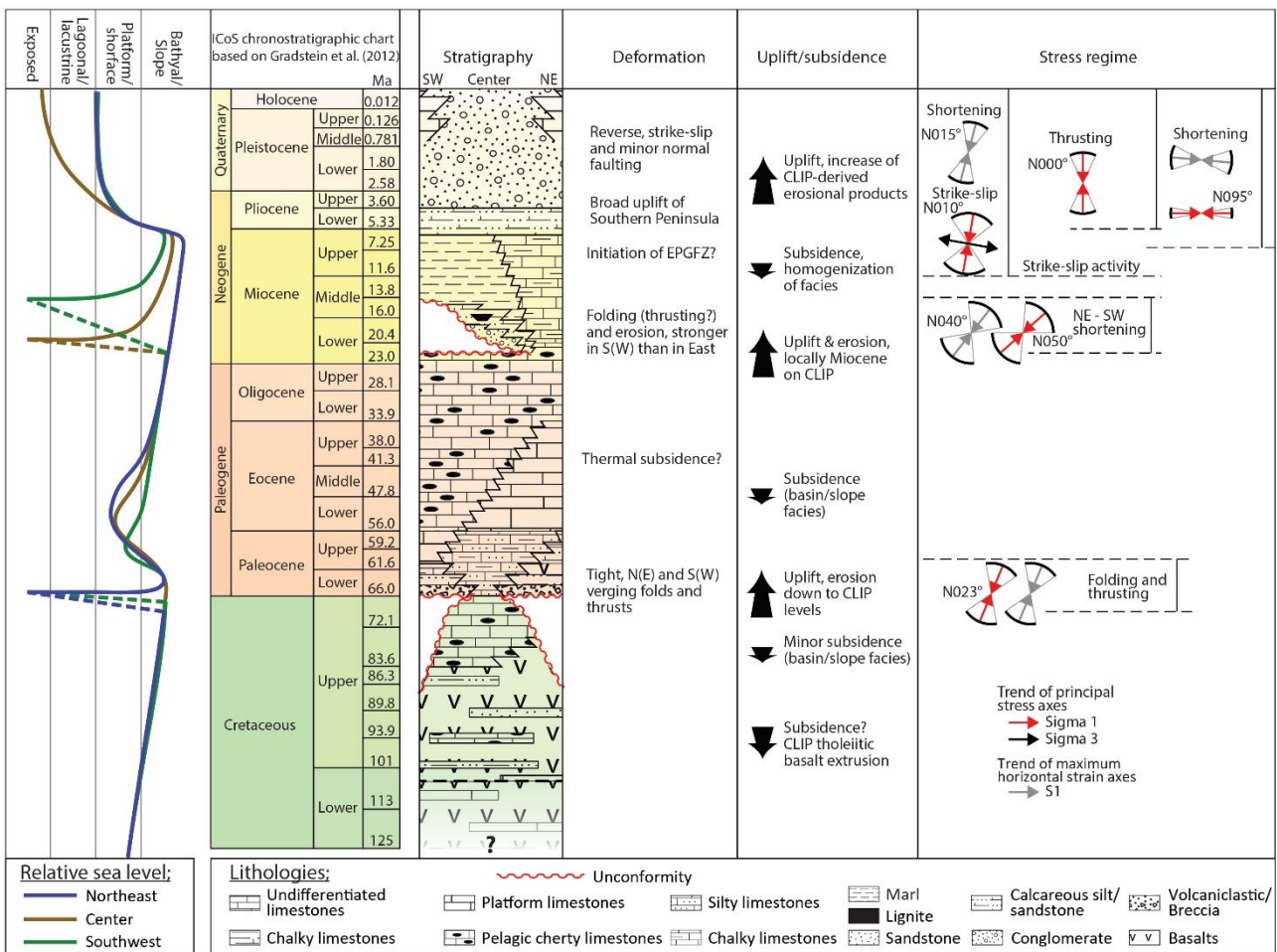


**Fig. 18:** Compilation chart for the Southern Peninsula displaying relative sea level, stratigraphy, deformation event, uplift and subsidence, and the associated stress regime. For discussion see text.



A dominant group of maximum principal stress axes is at a significantly high angle to the trace of the EPGFZ (Fig. 15b). The reverse regimes in the west are probably related to the Cretaceous – Paleocene deformation phase, as discussed in the first paragraph of this section. The reverse regimes observed in Miocene formations in the Massif de la Selle (Fig. 15a and Fig. 15b) post-date the early Miocene deformation phase, since this event did not considerably affect this region (Fig. 4b). The remainder of stresses that have a significantly high angle to the trace of the EPGFZ are related to a strike-slip stress regime (Fig. 15b). Present-day stresses, as recorded by the N021°E trend of the P-axis of the 2010 Léogâne earthquake, are at a 64° angle to the trace of the EPGFZ. This event did not involve slip on the EPGFZ (Prentice et al., 2010) however, but resulted from oblique slip on the NNW dipping Leogâne fault (Calais et al., 2010; Mercier de Lépinay et al., 2011; Douilly et al., 2013). Similar high angles of maximum principal stress are observed at the San Andreas Fault (SAF) system in California. There, the axis of maximum principal stress obtained from focal mechanisms, stress-induced wellbore breakouts and field measurements is also sub-perpendicular to the trace of the SAF, with fold axes and thrust faults trending sub-parallel to the trace (Zoback et al., 1987). These results are comparable with the data from the Cajon Pass (Zoback and Healy, 1992) and SAFOD (Hickman and Zoback, 2004) boreholes along the SAF, which in addition show considerable variation of the angular difference with depth. The high angle of  $\sigma_1$  to the trend of the SAF is interpreted as the result of stress rotations around a weak fault zone (Zoback et al., 1987). In similar fashion, the 80° angular difference between maximum horizontal stress and the trace of the Median Tectonic Line and the Rokko-Awaji segment in Japan is also interpreted to result from stress rotations proximal to a weak fault zone (Famin et al., 2014). The sub-perpendicular trend of  $\sigma_1$  axes to the trace of the EPGFZ could also indicate that this strike-slip fault is mechanically weak.

The east – west trending topographic lineament originating at Les Irois in the Massif de la Hotte (Fig. 9) is morphologically less expressed than the EPGFZ, and possibly represents an inactive strike-slip fault segment. An east – west trending strike-slip fault zone without a morphological expression is observed on the plateau southwest of Miragoane (Fig. 2b; Bourgueil et al., 1988). Locally short-lived strike-slip

activity during the late Miocene is documented at Les Cayettes quarry (section 4.5.3). Present-day strike-slip activity is mainly focused on the active segments of the EPGFZ (Mann et al., 1983, 1995; Prentice et al., 2010). During the development of a fault system, displacement may progressively become focused onto newly linked fault segments, with activity terminating on smaller faults (Walsh et al., 2002). Such a process possibly played a role in the development of the EPGFZ. In this scenario initially distributed strike-slip activity progressively became focused through time along the morphologically well express but strongly segmented EPGFZ, with activity terminating on older fault segments at a distance from the EPGFZ.

From the above discussion it follows that; 1) strike-slip activity became established during the late Miocene (Fig. 18) and was characterized by spatially distributed deformation, which 2) became progressively more focused along the EPGFZ from the latest Miocene or Pliocene onwards, possibly concomitant with EPGFZ-parallel shortening and compression, while 3) N – S directed thrusting, which locally post-dates strike-slip activity, became active from the Pliocene onwards.

### ***5.5 Structural style of deformation***

The Southern Peninsula is a large anticlinorium bounded by offshore oblique thrusts towards the north and south (Fig. 19). The half-wavelength of this structure increases from 55 km in the west at cross section A, to around 70 km at cross section C, and 90 km at section D (Fig. 19). In the northwestern part of the Southern Peninsula the general trend of this anticlinorium is east – west (Fig. 19). Towards the southeast this trend progressively changes to a NW – SE orientation (Fig. 19). In the Dominican Republic, the structural trend in the Sierra de Bahoruco, which is the eastward continuation of the Massif de la Selle, also becomes progressively NW – SE oriented (Van den Berghe, 1983a). This change in trend from west to east and north to south is likely related to the indentation of the Southern Peninsula - Beata Ridge basement block into central Hispaniola, which started in Miocene times (Pubellier et al., 1991; Mauffret and Leroy, 1999). The first-order folds (brown axes, Fig. 19) have similar trends as the main anticlinorium and wavelengths between 15 and 30 km (Fig. 19). The axes of

these folds are displaced, but their structural trend not disrupted by, the EPGFZ. Only the trends of the second-order folds (blue axes, Fig. 19) are controlled by the EPGFZ as well as other, minor faults. This is evidenced by the sub-parallel trend of the second-order folds in proximity to the segments of the EPGFZ (Fig. 19). The wavelengths of these folds vary between 3 and 10 km. We interpret these second-order folds as being controlled by strike-slip and associated thrust faults, whose spacing and dip angles are responsible for the variations in fold wavelength and orientation. In our interpretation, these faults mainly penetrate the CLIP basalts and sedimentary intercalations and are rooted in the crust (Fig. 19), as opposed to shallow decollement structures. The first-order folds appear unrelated to the mapped faults (Fig. 19). The 15 to 30 km wavelength of these folds is in the same order of magnitude as the 16 to 30 km crustal thickness of the Southern Peninsula (Corbeau et al., 2017). This could indicate that these folds are not directly controlled by faults, but are the result of large-wavelength buckling of the crust itself in response to the regional stress regime. An anti-correlation exists between regions of high elevation and basins on the Southern Peninsula (Fig. 19). In the west the highest elevations are directly north of the EPGFZ with the basins located to the south, which is inverted in the eastern part (Fig. 19). The trend of these basins and highs is generally sub-parallel to the EPGFZ, suggesting a structural control by the EPGFZ. Although the EPGFZ is a relatively young fault, it has a strong control on the present-day topography of the Southern Peninsula.

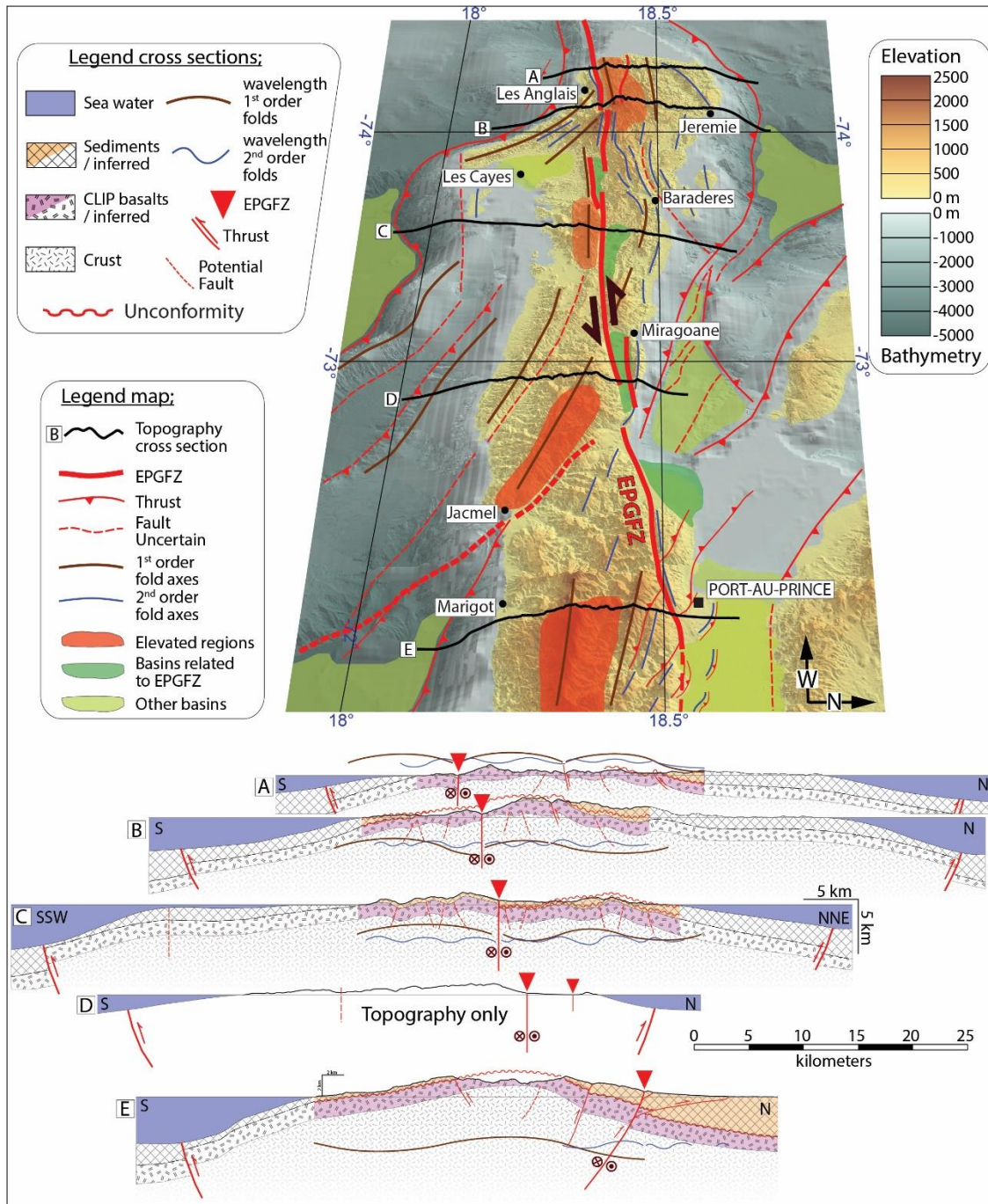


**Fig. 19:** Top map is a westwards facing perspective view of the Southern Peninsula. Background bathymetry is 30 arc-second interval data from GEBCO, high-resolution overlay bathymetry is at 25m resolution collected during the Haiti-SIS mission, onshore shaded relief is 30m resolution ASTER DEM. Elevation and bathymetry of the map are 2x exaggerated. Offshore faults modified from Bien-Aime Momplaisir (1986) and Mauffret and Leroy (1997) to match the bathymetry. Fold axes interpreted using the above data, the BME geological map (Fig. 2b) and our small-scale geological maps (Fig. 9, Fig. 11 and Fig. 13). Cross sections are on a 1-to-1 scale, with the relative spacing reflecting the distance between them: A and B are from the western Massif de la Hotte (A and B in Fig. 10), C is from the l'Asile region (C in Fig. 12), and E is from the Massif de la Selle (Fig. 14). For cross section D only the topography and the location of the major faults based on bathymetry and DEM is available, not the geology.

## ***5.6 Evolutionary cross section and regional implications***

The deformation phases described above are summarized in a series of schematic cross sections, illustrating the retro-deformation of the north-south cross section D of Fig. 12. The inferred amount of shortening shown in Fig. 20 is constructed using the line-length of the uppermost formation in the preceding image. This gives a conservative, minimum estimate of shortening between the Cretaceous and Present of ~11%, or ~2.3 km on this cross section. The total amount of shortening is probably larger due to overthrusting or layer-parallel shortening hidden by subsequent erosion.

- The top cartoon (Fig. 20a) shows the configuration at the end of the Cretaceous prior to the first deformation phase. Following emplacement of the Cretaceous flood basalts, pelagic sediments of the Macaya Formation were deposited. Intercalated sediments within the Cretaceous basalts and the Macaya Formation limestones indicate a general deepening trend from the Albian to Maastrichtian (Maurrasse et al., 1979; Bien-Aime Momplaisir, 1986; Bourgueil et al., 1988; Mann et al., 1991a).
- The first deformation phase (Fig. 20b) mainly occurred throughout the Maastrichtian, with minor deformation continuing into the early Paleocene. During this phase the Southern Peninsula was locally subjected to folding with S- to SW-vergence. Based on the extent of the erosional unconformity (Fig. 4a and Fig. 11) the first-order wavelength is estimated at around 20 km. This folding was probably aided by thrusts, similar to the one at Anse-d'Hainault (Fig. 9 and Fig. 10). Deformation in the l'Asile region (Fig. 11) resulted in erosion of the Cretaceous formations, which was more severe in the eastern part of this area. Maastrichtian erosion is also documented offshore southern Haiti on the northern Beata Ridge (Mauffret et al., 2001), while a Late Cretaceous deformation event is also recorded in the Blue Mountains of Jamaica (Mitchell, 2003, 2006; Abbott et al., 2013; West et al., 2014). Potential causes for this Maastrichtian to early Paleocene deformation are strongly related to the palinspastic position of the Southern Peninsula at that time. In the 'Pacific' origin models for the evolution of the



Caribbean by Pindell and Kennan (2009) the Southern Peninsula is located southeast of the deformation front that is bounding the Yucatan Peninsula to the south in the Maastrichtian. This deformation belt is characterized by south-verging structures, which matches the overall trend of south to southwest verging deformation on the Southern Peninsula at that time. In the 'autochthonous' origin models for the evolution of the Caribbean (Meschede and Frisch, 1998; James, 2006a; b) the Southern Peninsula remained in a relatively fixed position with respect to North and South America. This does not provide a clear candidate to explain the observed deformation during the Maastrichtian to early Paleocene on the Southern Peninsula. The exact palinspastic position during this period is however not very well constrained (Pindell and Kennan, 2009; Boschman et al., 2014). To resolve the cause of deformation a higher resolution palinspastic reconstruction of the northern Caribbean is needed.

- Subsidence and a deepening of facies characterized the late Paleocene to Aquitanian period (Fig. 20c). The global rise in sea level during this period of around 100m (Haq et al., 1988) is insufficient to account for the relative sea level rise and thickness of Paleogene sediments, which is at least 1000m (Bourgueil et al., 1988). Regional controls on the subsidence could involve: 1) a flexural response to deformation in the north, 2) a response to rifting and subsequent spreading in the Cayman Trough, or 3) cooling and contraction of the lithosphere following the Late Cretaceous flood basalt event, as proposed for other LIPs (Greene et al., 2010).
- Renewed folding and uplift during early Miocene times was more pronounced in the central region of the section (Fig. 20d). Erosion locally removed 500 to 1000m of Paleogene sediments. Tectonic inversion was possibly aided by reactivation of older faults. The cause for this deformation event remains enigmatic. The Oligocene to early Miocene corresponds to a number of major tectonic events in the region: 1) at a large scale, convergence between North and South America accelerated during the Oligocene resulting in increased compressional

deformation along the Caribbean Plate boundaries (Somoza, 2007), 2) the Cayman spreading center grew south between 26 and 20 Ma, which initiated activity on the Walton Fault (Leroy et al., 2000), 3) Hispaniola started to separate from Cuba at around 20 Ma (Pindell and Barrett, 1990; Calais and Mercier de Lépinay, 1995), contemporaneous with forward propagating folding and thrusting in central Haiti (Pubellier et al., 2000) and deformation at the Beata Ridge offshore southern Haiti (Mauffret and Leroy, 1999). The deformation observed onshore the Southern Peninsula during the late Oligocene – early Miocene is therefore possibly related to increased compression in the northern Caribbean realm.

- Renewed subsidence started in the Burdigalian and lasted until the Messinian (Fig. 20e). The l'Asile Basin became progressively deeper, with lacustrine and lagoonal sedimentation in the Burdigalian giving way to marine conditions that dominated from the Langhian onwards. The arrest of compressive deformation on the Southern Peninsula is possibly related to the initiation of the Septentrional – Oriente fault system, along which Hispaniola separated from Cuba from 20 Ma onwards (Pindell and Barrett, 1990; Calais and Mercier de Lépinay, 1995). The eastward escape of Hispaniola shifted the area of compressional deformation from the Southern Peninsula to the Haitian Fold-and-Thrust belt in the north.

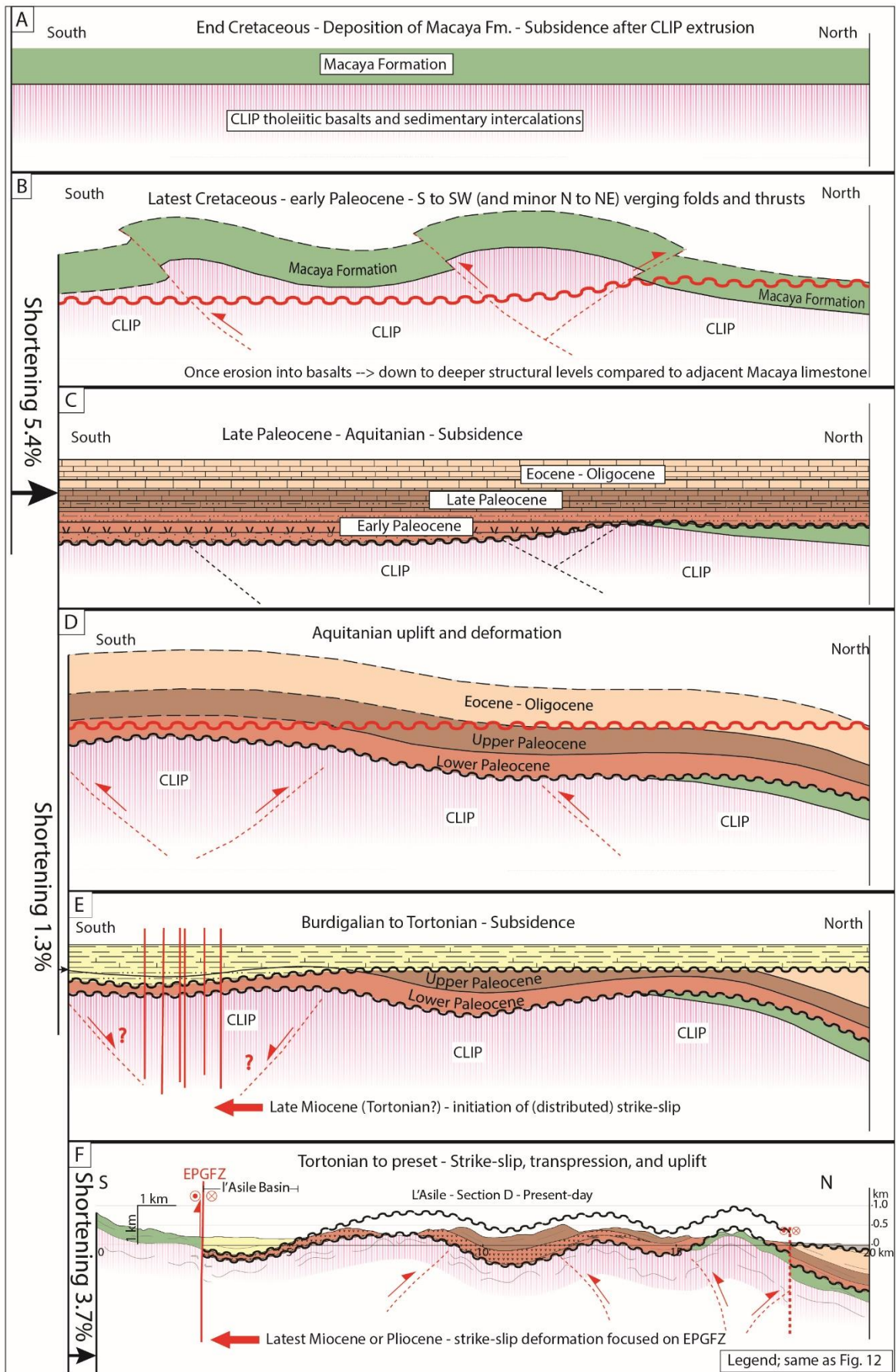


**Fig. 20:** Schematic evolutionary cross section through the l'Asile Basin, based on cross section D from Fig. 12d. The location of this cross section is shown on Fig. 11.

- Distributed strike-slip activity started during the late Miocene (Fig. 20e), which became focused along the present-day EPGFZ in the latest Miocene or Pliocene (Fig. 20f). A late Miocene timing for the onset of strike-slip activity along the EPGFZ is also found in Jamaica, which is recorded by the inversion of older Paleocene rift-related basins (Abbott et al., 2013; James-Williamson et al., 2014; Cochran et al., 2017). Strike-slip deformation became progressively more transpressive during the late Miocene, which resulted in uplift and shortening of the l'Asile Basin. Uplift is documented by a shallowing of facies and by erosion cutting down to the Cretaceous basalts during the Messinian. CLIP-derived erosion products are re-deposited in sediments from the Pliocene onwards. For the Southern Peninsula as a whole, our results indicate an increase in transpressive deformation from west to east, which also increases with time. Our results fit very well with the results from Corbeau et al. (2016a; b), who show very little to no transpressional deformation in the offshore domain between Jamaica and Haiti, and the results of Wang et al. (2018), who illustrate the presence of transpressive structures in the eastern Southern Peninsula and Sierra de Bahoruco in the Dominican Republic. Present-day deformation, as shown by GPS velocity models, also indicates an increase in fault-perpendicular compression from west to east over the Southern Peninsula (Benford et al., 2012a; Calais et al., 2016). This increase in transpressive deformation, both through time and from west to east on the Southern Peninsula is, on a regional scale, probably related to increased collision between northern Hispaniola and the Bahamas platform (Mann et al., 2002) and to the indentation of the Beata Ridge (Mauffret and Leroy, 1999). This resulted in a southwest-ward migration of the deformation front of the Haitian Fold-and-Thrust belt from the early Miocene onwards (Pubellier et al., 2000). Over time, this NW-SE trending deformation front affected the east-west trending Southern Peninsula more strongly in the east compared to the west, which is reflected by the resulting deformation as described in this paper.

## 6. Conclusions

The Cenozoic tectonic history of the Haitian Southern Peninsula is polyphase and we distinguish three major tectonic events.

1. **Deformation and uplift during the Maastrichtian to early Paleocene.** This deformation event is expressed by crustal-scale folds that developed coeval with predominantly south or southwest verging thrusts. Associated uplift caused partial erosion of the Upper Cretaceous sedimentary cover and of the CLIP basalts in large parts of the Southern Peninsula. Deformation resulted from NNE-directed compression. Following this deformation phase the Southern Peninsula experienced general subsidence and a transgressive period, associated with a deepening of depositional facies that continued until the Aquitanian.
2. **Deformation and uplift in the early Miocene.** This deformation phase mainly affected the southwestern parts of the Southern Peninsula. It is characterized by an eastwards decrease in uplift and erosion, and is not expressed in the eastern Southern Peninsula. Uplift resulted from NE – SW shortening and contemporaneous folding, which was possibly aided by reactivation of older thrusts in the western part of the peninsula. The depositional environment from the Burdigalian onwards is characterized by transgressive facies and a return to marine conditions, which lasted until the Messinian.
3. **Strike-slip followed by transpressional activity from late Miocene to recent.** Strike-slip activity along the EPGFZ started in the late Miocene (see section 5.3). Deformation was initially distributed and became progressively more focused along the EPGFZ from the Messinian or Pliocene onwards. This process created a new plate boundary which separated the Gonâve microplate from the Caribbean plate. The paleo-  $\sigma_1$  principal stress axis was sub-perpendicular to the EPGFZ during the late Miocene to Present-day, indicating that the fault zone is mechanically weak. Initial strike-slip motion along the EPGFZ became more transpressive



through time. This transpressional phase is recorded by 1) uplift of the Southern Peninsula from the Messinian onwards, 2) an increase in compressional deformation from West to East, which is manifested by 3) a change in structural style along the EPGFZ, with predominantly strike-slip faults in the west and oblique-slip faults in the east. The latter is also reflected by present-day GPS velocity models for the region, which show increased transpression from west to east. In the Massif de la Selle thrust faults developed from the Pliocene onwards. These faults are spatially associated with the EPGFZ and are probably rooted on this dominant fault zone at depth.

### **Acknowledgements**

The authors are grateful to the Bureau de Mines et de l'Énergie d'Haïti (BME) and the Université d'État d'Haïti (UEH) for providing invaluable support during the field campaigns. We want to thank Paul Mann and Manuel Pubellier for their reviews which helped improve the manuscript. This work greatly benefitted from an IFPEn internal report on the structure and stratigraphy of Haiti.

## References

- Abbott, R.N., Bandy, B.R., and Rajkumar, A., 2013: Cenozoic burial metamorphism in eastern Jamaica. *Caribbean Journal of Earth Science*, 46, 13–30.
- Ali, S.T., Freed, A.M., Calais, E., Manaker, D.M., and McCann, W.R., 2008: Coulomb stress evolution in Northeastern Caribbean over the past 250 years due to coseismic, postseismic and interseismic deformation. *Geophysical Journal International*, 174 (3), 904–918.
- Amilcar, H., 1997: Etude géologique du Massif de La Hotte occidentale, Presqu'île du Sud d'Haïti (Grandes Antilles). Implications géodynamiques: 188 p.
- Anderson, E.M., 1905: The dynamics of faulting. *Transactions of the Edinburgh Geological Society*, 8, 387–402.
- Ayala, A., 1959: Estudios de algunos microfósiles planctónicos de las calizas del Cretácico superior de la República de Haití. *Paleontología Mexicana*, 4, 42.
- Bakun, W.H., Flores, C.H., and ten Brink, U.S., 2012: Significant Earthquakes on the Enriquillo Fault System, Hispaniola, 1500-2010: Implications for Seismic Hazard. *Bulletin of the Seismological Society of America*, 102 (1), 18–30.
- Benford, B., DeMets, C., and Calais, E., 2012a: GPS estimates of microplate motions, northern Caribbean: evidence for a Hispaniola microplate and implications for earthquake hazard. *Geophysical Journal International*, 191 (2), 481–490.
- Benford, B., Tikoff, B., and DeMets, C., 2012b: Character of the Caribbean-Gôlave-North America plate boundaries in the upper mantle based on shear-wave splitting. *Geophysical Research Letters*, 39 (24), 1–6.
- Benford, B., Tikoff, B., and DeMets, C., 2015: Fault interaction of reactivated faults within a restraining bend: Neotectonic deformation of southwest Jamaica. *Lithosphere*, 7 (1), 21–39.
- Van den Berghe, B., 1983a: Evolution sédimentaire et structurale depuis le Paleocène du secteur "Massif de la Selle" (Haïti) - "Bahoruco" (République Dominicaine) au nord de la ride de Beata, dans l'orogène nord Caraïbe (Hispaniola-Grandes Antilles): 305 p.
- Van den Berghe, B., 1983b: Decrochement senestre sud-Haïtien : Analyses structurales dans le Massif de la Selle. *Ann. Soc. Géol. Nord*, 103, 317–323.
- Bien-Aime Momplaisir, R., 1986: Contribution à l'étude géologique de la partie orientale du Massif de la Hotte (Presqu'île du Sud d'Haïti); Synthèse structurale des marges de la Presqu'île à partir des données sismiques: 261 p.
- Bien-Aime Momplaisir, R., Amilcar, H., Murat Pierre, G., and Cenatus Amilcar, H., 1988: Les Cayes 1:250 000 geological map sheet.
- Bilham, R., 2010: Invisible faults under shaky ground. *Nature Geoscience*, 3 (11), 743–745.
- Bizon, G., Bizon, J.J., Calmus, T., Muller, C., and Van den Berghe, B., 1985: Stratigraphie du Tertiaire du sud d'Hispaniola (Grandes Antilles). Influence de la tectonique déchrochante sur la paléogéographie et l'histoire sédimentaire. *Symp. Geodyn. Caraïbes, Paris, Ed. Technip*, 371–380.
- Boisson, D., and Bien-Aime Momplaisir, R., 1987: Port-au-Prince 1:250 000 geological map sheet. , 1.
- Boschman, L.M., van Hinsbergen, D.J.J., Torsvik, T.H., Spakman, W., and Pindell, J.L., 2014: Kinematic reconstruction of the Caribbean region since the Early Jurassic. *Earth-Science Reviews*, 138, 102–136.
- BouDagher-Fadel, M.K., 2008: Evolution and Geological significance of Larger Benthic Foraminifera. *Elsevier B.V.*, 1-547.
- BouDagher-Fadel, M.K., 2015: Biostratigraphic and Geological Significance of Planktonic Foraminifera. *UCLpress*, 1-320.
- Bourgeois, B., Andreieff, P., Lasnier, J., Gonnard, R., Le Métour, J., and Rançon, J.-P., 1988: Synthèse géologique de la République d'Haïti, in Technical report- ATN/SF 2506 HA, Port-au-Prince, *Bureau des Mines et de l'Énergie d'Haïti*, 332.
- Butterlin, J., 1954: La géologie de la République d'Haïti et ses rapports avec celle des régions voisines. *Publ. Comité 150<sup>ème</sup> Anniv. Indépendance, P-Au-P.*, 446.
- Butterlin, J., 1960: Géologie générale et régionale de la République d'Haïti. *Univ. Paris, Travaux Mém. Inst. Htes. Etud. Amér. Latine, VI*, 194.
- Calais, E., and Mercier de Lépinay, B., 1995: Strike-Slip Tectonic Processes in the Northern Caribbean Between Cuba and Hispaniola (Windward Passage). *Marine Geophysical Researches*, 17, 63–95.
- Calais, E., Freed, A., Mattioli, G., Amelung, F., Jónsson, S., Jansma, P., Hong, S.-H., Dixon, T., Prépetit, C., and Momplaisir, R., 2010: Transpressional rupture of an unmapped fault during the 2010 Haiti earthquake. *Nature Geoscience*, 3 (11), 794–799.
- Calais, E., Symithe, S., Mercier de Lépinay, B., and Prépetit, C., 2016: Plate boundary segmentation in the northeastern Caribbean from geodetic measurements and Neogene geological observations. *C.R. Geoscience*, 348, 42–51.
- Calmus, T., 1983: Contribution à l'étude géologique du Massif de Macaya (Sud-ouest d'Haïti, Grandes Antilles). Sa place dans l'évolution de l'orogène Nord-Caraïbe: Université Pierre et Marie Curie, 222 p.
- Calmus, T., 1984: Decrochement senestre sud-Haïtien: Analyses et conséquences paléogéographiques dans la région de Camp-Perrin (Massif de Macaya, Presqu'île du sud d'Haïti). *Ann. Soc. Géol. Nord*, 103, 309–316.
- Calmus, T., 1987: Études géochimiques des volcanismes crétacé et Tertiaire du Massif de Macaya (presqu'île du Sud d'Haïti): Leur place dans l'évolution tectonique de la région nord-caraïbe. *C.R. Ac. Sc., Paris, II* (16), 981–986.
- Calmus, T., and Vila, J.-M., 1988: The Massif de Macaya (Haïti): the evolution of a Laramide structure in the left-handed-strike-slip boundary between North-America and Caribbean Plates. *Bol. Depto. Geol. Uni-Son.*, 5 (1), 63–69.
- Cochran, W.J., Spotila, J.A., Prince, P.S., and McAleer, R.J., 2017: Rapid exhumation of Cretaceous arc-rocks along the Blue Mountains restraining bend of the Enriquillo-Plantain Garden fault, Jamaica, using thermochronometry from multiple closure systems. *Tectonophysics*, 721, 292–309.

- Corbeau, J., Rolandone, F., Leroy, S., Mercier de Lépinay, B., Meyer, B., Ellouz-Zimmermann, N., and Momplaisir, R., 2016a: The northern Caribbean plate boundary in the Jamaica Passage: Structure and seismic stratigraphy. *Tectonophysics*, 675, 209–226.
- Corbeau, J., Rolandone, F., Leroy, S., Meyer, B., and Mercier de Lépinay, B Momplaisir, R., 2016b: How transpressive is the northern Caribbean plate boundary? *Tectonics*, 35, 1032–1046.
- Corbeau, J., Rolandone, F., Leroy, S., Guerrier, K., Keir, D., Stuart, G., Clouard, V., Gallacher, R., Ulysse, S., Boisson, D., Momplaisir, R., Saint Preux, F., Prépetit, C., Saurel, J., et al., 2017: Crustal structure of western Hispaniola (Haiti) from a teleseismic receiver function study. *Tectonophysics*, 709, 9–19.
- DeMets, C., Gordon, R.G., and Argus, D.F., 2010: Geologically current plate motions. *Geophysical Journal International*, 181 (1), 1–80.
- Desreumaux, C., 1985a: Haïti: Un modele recent et actuel de systeme compressif a effet centripete. *Géodynamique des Caraïbes, ed. Technip, Paris,*, 391–402.
- Desreumaux, C., 1985b: Sur la presence d'une serie carbonatee contiue de type bassin Caraïbe du Cretace terminal au Miocene dans la Presqu'île du sud d'Haïti, Grandes Antilles. *C. R. Ac. Sc., Paris*, 5 (II), 319–322.
- Desreumaux, C., 1987: Contribution a l'étude de l'histoire geologique des regions centrale et meridional d'Haïti (Grandes Antilles) du Cretace à l'actuel: 507 p.
- Díaz de Neira, J.A., 2002: Geomorphologic evolution of the Llano de Azua (South of the Dominican Republic). *Acta Geologica Hispanica*, 37 (2–3), 207–227.
- Douilly, R., Haase, J.S., Ellsworth, W.L., Bouin, M.-P., Calais, E., Symithe, S.J., Armbruster, J.G., Mercier de Lépinay, B., Deschamps, A., Mildor, S.-L., Meremonte, M.E., and Hough, S.E., 2013: Crustal structure and fault geometry of the 2010 Haiti earthquake from temporary seismometer deployments. *Bulletin of the Seismological Society of America*, 103 (4), 2305–2325.
- Duplan, L., 1975: Etude photogéologique de la région sud de la République d'Haïti (Nations-Unies), projet de développement minier.
- Famin, V., Raimbourg, H., Garcia, S., Bellahsen, N., Hamada, Y., Boullier, A.M., Fabbri, O., Michon, L., Uchide, T., Ricci, T., Hirono, T., and Kawabata, K., 2014: Stress rotations and the long-term weakness of the Median Tectonic Line and the Rokko-Awaji Segment. *Tectonics*, 33 (10), 1900–1919.
- Fossen, H., 2010: Structural Geology. *Cambridge University Press*, 463.
- Gradstein, F.M., Ogg, J.G., Schmitz, J., and Ogg, G., 2012: The Geologic Time Scale 2012. *Elsevier*, 1176.
- Greene, A.R., Scoates, J.S., Weis, D., Katvala, E.C., and Nixon, G.T., 2010: The architecture of oceanic plateaus revealed by the volcanic stratigraphy of the accreted Wrangellia oceanic plateau. *Geosphere*, 6 (1), 47–73.
- Haq, B.U., Hardenbol, J., and Vail, P.R., 1988: Mesozoic and Cenozoic chronostratigraphy and cycles of sea-level change. *Science*, 241, 71–108.
- Hayes, G.P., Briggs, R.W., Sladen, a., Fielding, E.J., Prentice, C., Hudnut, K., Mann, P., Taylor, F.W., Crone, a. J., Gold, R., Ito, T., and Simons, M., 2010: Complex rupture during the 12 January 2010 Haiti earthquake. *Nature Geoscience*, 3 (11), 800–805.
- Heubeck, C., and Mann, P., 1991: Geologic evaluation of plate kinematic models for the North American-Caribbean plate boundary zone. *Tectonophysics*, 191, 1–26.
- Hickman, S., and Zoback, M., 2004: Stress orientations and magnitudes in the SAFOD pilot hole. *Geophysical Research Letters*, 31 (15), 13–16.
- Hilgen, F.J., Lourens, L.J., Van Dam, J.A., Beu, A.G., Boyes, A.F., Cooper, R.A., Krijgsman, W., Ogg, J.G., Piller, W.E., and Wilson, D.S., 2012: The Neogene Period, in Gradstein, F.M., Ogg, J.G., Schmitz, M.D., and Ogg, G.M. eds., *The Geologic Time Scale*, Boston, *Elsevier*, 923–978.
- Hornbach, M.J., Braudy, N., Briggs, R.W.R.W., Cormier, M.-H.M.-H., Davis, M.B.M.B., Diebold, J.B.J.B., Dieudonne, N., Douilly, R., Frohlich, C., Gulick, S.P.S.S.P.S., Johnson III, H.E.H.E., Mann, P., McHugh, C., Ryan-Mishkin, K., et al., 2010: High tsunami frequency as a result of combined strike-slip faulting and coastal landslides. *Nature Geoscience*, 3 (11), 783–788.
- International Seismological Centre, 2014: On-line Bulletin. <http://www.isc.ac.uk>.
- James, K.H., 2006a: Arguments for and against the Pacific origin of the Caribbean Plate: discussion, finding for an inter-American origin. *Geologica Acta*, 4 (1–2), 279–302.
- James, K.H., 2006b: The Caribbean Ocean Plateau – an overview, and a different understanding. , 1–28.
- James-Williamson, S.A., Mitchell, S.F., and Ramsook, R., 2014: Tectono-stratigraphic development of the Coastal Group of south-eastern Jamaica. *Journal of South American Earth Sciences*, 50, 40–47.
- Kerr, A.C., White, R. V, Thompson, P.M.E., and Saunders, A.D., 2003: No Oceanic Plateau — No Caribbean Plate? The seminal role of an Oceanic Plateau in Caribbean plate evolution. *AAPG Memoir*, 79, 126–168.
- Kroehler, M.E., Mann, P., Escalona, A., and Christeson, G.L., 2011: Late Cretaceous-Miocene diachronous onset of back thrusting along the South Caribbean deformed belt and its importance for understanding processes of arc collision and crustal growth. *Tectonics*, 30 (6), 1–31.
- Leroy, S., 1995: Structure et origine de la Plaque Caraïbe: Implications géodynamiques: Université Pierre et Marie Curie - Paris 6, 230 p.
- Leroy, S., Mauffret, A., Patriat, P., and Mercier de Lépinay, B., 2000: An alternative interpretation of the Cayman trough evolution from a reidentification of magnetic anomalies. *Geophysical Journal International*, 141 (3), 539–557.
- Leroy, S., Ellouz-Zimmermann, N., Corbeau, J., Rolandone, F., Mercier de Lépinay, B., Meyer, B., Momplaisir, R., Granja

- Bruña, J.L., Battani, A., Baurion, C., Burov, E., Clouard, V., Deschamps, R., Gorini, C., et al., 2015: Segmentation and kinematics of the North America-Caribbean plate boundary offshore Hispaniola. *Terra Nova*, 27 (6), 467–478.
- Mann, P., Hempton, M.R., Bradley, D.C., and Burke, K., 1983: Development of Pull-Apart Basins. *The Journal of Geology*, 91 (5), 529–554.
- Mann, P., and Burke, K., 1984: Neotectonics of the Caribbean. *Reviews of geophysics and space physics*, 22 (4), 309–362.
- Mann, P., Draper, G., and Lewis, J.F., 1991a: An overview of the geologic and tectonic development of Hispaniola. *Geological Society of America Special Paper*, 262, 1–27.
- Mann, P., McLaughlin, P.P., and Cooper, C., 1991b: Geology of the Azua and Enriquillo basins, Dominican Republic; 2, Structure and tectonics. *Geological Society of America Special Paper*, 262, 367–389.
- Mann, P., Taylor, F.W., Edwards, R.L., and Ku, T.-L., 1995: Actively evolving microplate formation by oblique collision and sideways motion along strike-slip faults: An example from the northeastern Caribbean plate margin. *Tectonophysics*, 246 (1–3), 1–69.
- Mann, P., Calais, E., Ruegg, J.-C., DeMets, C., Jansma, P.E., and Mattioli, G.S., 2002: Oblique collision in the northeastern Caribbean from GPS measurements and geological observations. *Tectonics*, 21 (6), 1–26.
- Mauffret, A., and Leroy, S., 1997: Seismic stratigraphy and structure of the Caribbean igneous province. *Tectonophysics*, 283 (1–4), 61–104.
- Mauffret, A., and Leroy, S., 1999: Neogene Intraplate Deformation of the Caribbean Plate at the Beata Ridge, in Mann, P. ed., *Sedimentary Basins of the World; Caribbean Basins*, Amsterdam, Elsevier Science B.V., 627–669.
- Mauffret, A., Leroy, S., Vila, J., Hallot, E., L, B.M. De, and Duncan, R.A., 2001: Prolonged Magmatic and Tectonic Development of the Caribbean Igneous Province Revealed by a Diving Submersible Survey. *Marine Geophysical Researches*, 22, 17–45.
- Maurrasse, F., Husler, J., Georges, G., Schmitt, R., and Damond, P., 1979: Upraised Caribbean seafloor below acoustic reflector B" at the Southern Peninsula of Haiti. *Geologie en Mijnbouw*, 58 (1), 71–83.
- Maurrasse, F., 1980: New data on the stratigraphy of the Southern Peninsula of Haïti. *1 ère Coll. Géologie d'Haïti, Impr. Le Natal, P-au-P.*, 184–198.
- Maurrasse, F., 1982: Survey of the geology of Haïti: Guide to the field excursions in Haïti. *Miami Geological Society*, 103.
- Maurrasse, J.-M.R.F., and Sen, G., 1991: Impacts, Tsunamis, and the Haitian Cretaceous-Tertiary Boundary Layer. *Science*, 252 (5013), 1690–1693.
- McCann, W.R., 2006: Estimating the threat of tsunamigenic earthquakes and earthquake induced-landslide tsunami in the Caribbean, in Aurelio, M. and Philip, L. eds., *Caribbean Tsunami Hazard*, World Scientific Publishing, Singapore, 43–65.
- McLaughlin, P.P., and Sen Gupta, B.K., 1991: Migration of Neogene marine environments, southwestern Dominican Republic. *Geology*, 19 (3), 222–225.
- Mercier de Lépinay, B., Labesse, B., Sigal, J., and Vila, J.M., 1979: Sedimentation chaotique et tectonique tangentielle Maestrichtienne dans la Presqu'île du Sud d'Haïti (île d'Hispaniola, Grandes Antilles). *C.R. Ac. Sc. Paris*, 289 (D), 887–890.
- Mercier de Lépinay, B., Deschamps, A., Klingelhoefer, F., Mazabraud, Y., Delouis, B., Clouard, V., Hello, Y., Crozon, J., Marcaillou, B., Graindorge, D., Vallée, M., Perrot, J., Bouin, M.-P., Saurel, J.-M., et al., 2011: The 2010 Haiti earthquake: A complex fault pattern constrained by seismologic and tectonic observations. *Geophysical Research Letters*, 38 (L22305), 1–7.
- Meschede, M., and Frisch, W., 1998: A plate-tectonic model for the Mesozoic and Early Cenozoic history of the Caribbean plate. *Tectonophysics*, 296 (3–4), 269–291.
- Mitchell, S.F., 2003: Sedimentology and tectonic evolution of the Cretaceous rocks of Central Jamaica: Relationships to the plate tectonic evolution of the Caribbean. *AAPG Memoir*, 79, 605–623.
- Mitchell, S.F., 2006: Timing and implications of Late Cretaceous tectonic and sedimentary events in Jamaica. *Geologica Acta*, 4 (1–2), 171–178.
- Ogg, J.G., Hinnov, L.A., and Huang, C., 2012: Cretaceous, in Gradstein, F.M., Ogg, J.G., Schmitz, J., and Ogg, G.M. eds., *The Geologic time Scale*, Boston, Elsevier, 793–853.
- Pindell, J.L., and Barrett, S.F., 1990: Geological evolution of the Caribbean region: A plate tectonic perspective, in Dengo, G. and Case, J.E. eds., *The Geology of North America - Vol. H, The Caribbean Region*, Boulder, Geological Society of America, 405–433.
- Pindell, J.L., and Kennan, L., 2009: Tectonic evolution of the Gulf of Mexico, Caribbean and northern South America in the mantle reference frame: an update, in James, K.H., Lorente, M.A., and Pindell, J.L. eds., *The Origin and Evolution of the Caribbean Plate*, Geological Society, London, Special Publications, 328, 1–55.
- Prentice, C.S., Mann, P., Crone, a. J., Gold, R.D., Hudnut, K.W., Briggs, R.W., Koehler, R.D., and Jean, P., 2010: Seismic hazard of the Enriquillo–Plantain Garden fault in Haiti inferred from palaeoseismology. *Nature Geoscience*, 3 (11), 789–793.
- Pubellier, M., Vila, J.-M., and Boisson, D., 1991: North Caribbean neotectonic events: The Trans-Haitian fault system. Tertiary record of an oblique transcurrent shear zone uplifted in Hispaniola. *Tectonophysics*, 194 (3), 217–236.
- Pubellier, M., Mauffret, A., Leroy, S., Vila, J.-M., and Amilcar, H., 2000: Plate boundary readjustment in oblique convergence: Example of the Neogene of Hispaniola, Greater Antilles. *Tectonics*, 19 (4), 630–648.
- Rosencrantz, E., and Mann, P., 1991: SeaMARC II mapping of transform faults in the Cayman Trough, Caribbean Sea. *Geology*, 19, 690–693.

- Saint-Fleur, N., Feuillet, N., Grandin, R., Jacques, E., Weil-Accardo, J., and Klinger, Y., 2015: Seismotectonics of southern Haiti: A new faulting model for the 12 January 2010 M7.0 earthquake. *Geophysical Research Letters*, 42 (23), 10273–10281.
- Simpson, R.W., 1997: Quantifying Anderson's fault types. *Journal of Geophysical Research: Solid Earth*, 102 (B8), 17909–17919.
- Sinton, C.W., Duncan, R.A., Storey, M., Lewis, J., and Estrada, J.J., 1998: An oceanic flood basalt province within the Caribbean plate. *Earth and Planetary Science Letters*, 155, 221–235.
- Somoza, R., 2007: Eocene paleomagnetic pole for South America: Northward continental motion in the Cenozoic, opening of Drake Passage and Caribbean convergence. *Journal of Geophysical Research: Solid Earth*, 112 (3), 1–11.
- Symithe, S.J., Calais, E., Haase, J.S., Freed, A.M., and Douilly, R., 2013: Coseismic slip distribution of the 2010 M 7.0 Haiti earthquake and resulting stress changes on regional faults. *Bulletin of the Seismological Society of America*, 103 (4), 2326–2343.
- Symithe, S.J., Calais, E., de Chabaliere, J.B., Robertson, R., and Higgins, M., 2015: Current block motions and strain accumulation on active faults in the Caribbean. *Journal of Geophysical Research: Solid Earth*, 120, 1–27.
- Symithe, S., and Calais, E., 2016: Present-day shortening in Southern Haiti from GPS measurements and implications for seismic hazard. *Tectonophysics*, 679, 117–124.
- Terrier, M., Bialkowski, A., Nachbaur, A., Prépetit, C., Joseph, Y.F., and Joshph, Y.F., 2014: Revision of the geological context of the Port-au-Prince metropolitan area, Haiti: Implications for slope failures and seismic hazard assessment. *Natural Hazards and Earth System Sciences*, 14 (9), 2577–2587.
- Twiss, R.J., and Moores, E.M., 2007: Structural geology. 742.
- Vandenbergh, N., Hilgen, F.J., Speijer, R.P., Ogg, J.G., Gradstein, F.M., Hammer, O., Hollis, C.J., and Hooker, J.J., 2012: The Paleogene Period, in Gradstein, F.M., Ogg, J.G., Schmitz, M.D., and Ogg, G.M. eds., *The Geologic Time Scale*, Boston, Elsevier, 855–921.
- Walsh, J.J., Nicol, A., and Childs, C., 2002: An alternative model for the growth of faults. *Journal of Structural Geology*, 24, 1669–1675.
- Wang, J., Mann, P., and Stewart, R.R., 2018: Late Holocene Structural Style and Seismicity of Highly Transpressional Faults in Southern Haiti. *Tectonics*, 37, 1–19.
- Wessels, R.J.F., 2019: Strike-slip fault systems along the northern Caribbean plate boundary, in Duarte, J.C. ed., *Transform plate boundaries and fracture zones*, Elsevier, 375–395.
- West, D.P., Abbott, R.N., Bandy, B.R., and Kunk, M.J., 2014: Protolith provenance and thermotectonic history of metamorphic rocks in eastern Jamaica: Evolution of a transform plate boundary. *Geological Society of America Bulletin*, 126 (3–4), 600–614.
- Yamaji, A., Sato, K., and Otsubo, M., 2005: Multiple Inverse Method Software Package. *Division of Earth & Planetary Sciences, Kyoto University*, 1–16.
- Young, J.R., Bown, P.R., and Lees, J.A., 2018a: Nannotax3 website.
- Young, J.R., Wade, B.S., and Hubert, B.T., 2018b: Pforams@mikrotax website.
- Zoback, M.D., Zoback, M. Lou, Mount, V.S., Suppe, J., Eaton, J.P., Healy, J.H., Oppenheimer, D., Reasenber, P., Jones, L., Raleigh, C.B., Wong, I.G., Scotti, O., and Wentworth, C., 1987: New evidence on the state of stress of the San Andreas fault system. *Science*, 238 (4830), 1105–1111.
- Zoback, M.D., and Healy, J.H., 1992: In situ stress measurements to 3.5 km depth in the Cajon Pass Scientific Research Borehole: Implications for the mechanics of crustal faulting. *Journal of Geophysical Research*, 97 (B4), 5039.



## Figure captions

**Fig. 1a:** Geodynamic setting of the Caribbean. GPS velocities (black arrows) from DeMets et al. (2010) in a Caribbean reference frame. **Fig. 1b:** Geodynamic setting of Haiti. GPS velocity vectors (black arrows) from Calais et al. (2016). GPS velocity vectors indicate motion of block to the south (west) of fault with respect to block to the north (west). Faults modified after Leroy (1995). MCSC = Mid-Cayman Spreading Center; OFZ = Oriente Fault Zone; SDB = Santiago Deformed Belt; SFZ = Septentrional Fault Zone; NHDB = North Hispaniola Deformed Belt; HFTB = Haitian Fold-and-thrust belt; EPGFZ = Enriquillo-Plantain Garden Fault Zone; WFZ = Walton Fault Zone; D.R. = Dominican Republic; P.R. = Puerto Rico; V.I. = Virgin Islands; PRVI = Puerto Rico – Virgin Islands block. .... 3

**Fig. 2a:** Structural map of the Southern Peninsula. Onshore shaded relief is 30m resolution ASTER DEM, offshore bathymetry is at 25m resolution and was collected during the Haiti-SIS cruises (Leroy et al., 2015). Offshore faults from Bien-Aime Momplaisir (1986) and Leroy et al. (2015). Onshore structures from Mann et al. (1995), Saint Fleur et al. (2015), Symithe and Calais (2016). Dashed trace of EPGFZ represents interpretation by Wang et al. (2018). GPS velocity vectors constructed from Calais et al. (2016). Earthquake focal mechanisms from the International Seismological Centre (2014) (GCMT). **Fig. 2b:** Compilation and simplification of 1:250.000 geological maps published by the Bureau des Mines et de l'Energie d'Haiti (BME) after Boisson and Bien-Aime Momplaisir, 1987; Bien-Aime Momplaisir et al., 1988). Black rectangles show extent of small scale geological maps and corresponding figures. Black lines are cross sections. .... 5

**Fig. 3:** Synthetic stratigraphic column for the Southern Peninsula. Relative sealevel for northeast (blue), central (brown) and southwest (green). Data from references in text. Chronostratigraphic chart from the International Commission on Stratigraphy (ICoS) based on the geologic time scale from Gradstein et al. (2012). .... 8

**Fig. 4a:** Compilation map of the Cretaceous – Paleocene unconformity based on biostratigraphic ages for Paleocene deposits and underlying formations. Color coding indicates paleo-erosion. Red; strong, paleo-erosion down into Cretaceous basalts. Yellow; mild, paleo-erosion down into Cretaceous Macaya Formation limestones. Green; conformable, biostratigraphically complete and concordant transition from Cretaceous to Paleogene. **Fig. 4b:** Compilation map of the Cretaceous – Paleocene unconformity based on biostratigraphic ages for lower to middle Miocene deposits and underlying formations. Color coding indicates paleo-erosion. Red; strong, paleo-erosion down to Cretaceous. Orange; medium, paleo-erosion down to Paleocene or Eocene. Yellow; mild, paleo-erosion down to Oligocene or intra-Miocene. Green; conformable, biostratigraphically complete and concordant transition from Paleogene to Neogene. Present-day trace of the EPGFZ on both figures indicated in red. Dashed line represents interpretation by Wang et al. (2018). .... 16

**Fig. 5a:** Unconformable contact between CLIP basalts and calcareous clay-, silt- and sandstones of the lower Paleocene, overlain by upper Paleocene clastic limestones. Top of ridge consists of lower Eocene cherty limestones. Fig. 9; northwest of Morne La Visite. **Fig. 5b:** Unconformable contact between CLIP basalts and middle Miocene limestones. Haut Fort, south of Tiburon. .... 17

**Fig. 6a:** Boudinage of intercalated limestones within CLIP basalts. Location on Fig. 9; northwest of Les Anglais. **Fig. 6b:** Disharmonically folded Macaya Formation limestones with WNW-trending fold axes. Location on Fig. 9; Tiburon Valley. **Fig. 6c:** Lower Eocene platform limestone gently folded along ENE-trending fold axis. Location on Fig. 9; Tiburon Valley. **Fig. 6d:** North – south trending normal faults in middle Miocene chinks. Location on Fig. 9; NW of Port-a-Piment. .... 19

**Fig. 7a:** Thrust contact between Macaya Formation limestones and CLIP basalts. Contact is brecciated and underlying basalts are hydrothermally altered. Location on Fig. 11; SE of Mornes. **Fig. 7b:** Tight southwest verging folds within Paleocene calcarenites. Location on Fig. 11; SE of Mornes. .... 20

**Fig. 8a:** Fault with unknown sense of motion separating Eocene platform limestones from CLIP basalts. Location on Fig. 13; west of Obleon, northern flank of Massif de la Selle. **Fig. 8b:** Fault core of the EPGFZ. South-dipping, east – west trending fault mirrors. Location on Fig. 13; La Boule quarry. **Fig. 8c:** Southwest verging thrust separating upper Miocene – lower Pliocene marlstones in the footwall from lower to middle Miocene chalky limestones in the hanging wall. Location on Fig. 13; Les Cayettes quarry. .... 22

**Fig. 9:** Geological map of the Tiburon area. For location see **Fig. 2b**. Black bedding symbols with dip in degrees are measured in the field. Black fold axes represent folds constructed using outcrop measurements. Bedding symbols in grey are obtained using satellite imagery. Solid black lines are observed structures, dashed black lines denote structures from literature, while dashed grey lines are structures based on satellite image interpretation. .... 24

**Fig. 10:** One-to-one scale cross sections of the western Massif de la Hotte. Locations of cross sections in **Fig. 9**. The topography is derived using ASTER DEM data. Faults shown as solid red lines are observed while dashed red lines are from satellite interpretation. Grey lines within the formations denote the inferred general trend of the bedding, which schematically shows tighter folding in the Cretaceous formations compared to the Cenozoic formations. Only the large-scale structures are shown. Dip of EPGFZ unknown. Abbreviations; *App.* = *Appendix*, *EPGFZ* = *Enriquillo – Plantain Garden Fault Zone*. .... 25

**Fig. 11:** Geological map of the l'Asile area. For location see **Fig. 2b**. Symbols are the same as described in the caption of **Fig. 9**. .... 27

**Fig. 12:** One-to-one scale cross sections of the l'Asile Basin area. Locations in **Fig. 11**. Symbols are the same as described in the caption of **Fig. 10**. Dip of EPGFZ unknown. Tighter folding within the Cretaceous formations compared to the Cenozoic formations schematically represented. .... 28

**Fig. 13:** Geological map of the Marigot area. For location see **Fig. 2b**. Symbols are the same as described in the caption of **Fig. 9**. .... 31

**Fig. 14:** One-to-one scale cross section of the Massif de la Selle. Locations in **Fig. 13**. Symbols are the same as described in the caption of **Fig. 10**. Tighter folding within the Cretaceous formations compared to the Cenozoic formations schematically represented. .... 32

**Fig. 15a:** Plot of trends of sigma 1 (black) and sigma 3 (blue) axes from stress inversion results. Fold axes derived from outcrops are plotted in green. **Fig. 15b:** Chart showing angular difference (degrees) between trend of the sigma 1 or sigma 3 axes and the trace of the EPGFZ. Colors indicate age of lithologies from which the data was obtained. Square indicates normal stress regime, circle indicates strike-slip stress regime and hashed circle indicates reverse stress regime. Results on the right-hand side are constructed using the N095°E average trend of thrusts in this region. Red circle is data from the core of the EPGFZ. Plotted results are at less than 15km distance from the EPGFZ trace. Angular difference varies between -20 and +100 degrees (see inset on right). .... 36

**Fig. 16a:** Plot showing trend of sigma 1 axes vs distance to the trace of the EPGFZ for measurements within 15 km of this fault. Arrows indicate dominant trends. Measurements obtained from the fault core are within the red hashed zone. **Fig. 16b:** Same principle as figure 16a but for fold axes derived from outcrops. **Fig. 16c:** Comparison between groups A, B and C from averaged  $\sigma_1$  trend and averaged axes of contraction. .... 37

**Fig. 17:** Block cartoons showing the fault geometries corresponding to the different scenarios for the faults bordering the southern Cul-de-Sac plain. **Fig. 17a** and **Fig. 17b** correspond to scenario 1 as shown in **Fig. 14a**. **Fig. 17c** and **Fig. 17d** correspond to scenario 2 as shown in **Fig. 14b**. **Fig. 17e** is a simplified geological map from **Fig. 13**. Black box corresponds to the geographical extent of the block cartoons in Figs. 17a and 17c. .... 43

**Fig. 18:** Compilation chart for the Southern Peninsula displaying relative sea level, stratigraphy, deformation event, uplift and subsidence, and the associated stress regime. For discussion see text. .... 45

**Fig. 19:** Top map is a westwards facing perspective view of the Southern Peninsula. Background bathymetry is 30 arc-second interval data from GEBCO, high-resolution overlay bathymetry is at 25m resolution collected during the Haiti-SIS mission, onshore shaded relief is 30m resolution ASTER DEM. Elevation and bathymetry of the map are 2x exaggerated. Offshore faults modified from Bien-Aime Momplaisir (1986) and Mauffret and Leroy (1997) to match the bathymetry. Fold axes interpreted using the above data, the BME geological map (Fig. 2b) and our small-scale geological maps (Fig. 9, Fig. 11 and Fig. 13). Cross sections are on a 1-to-1 scale, with the relative spacing reflecting the distance between them: A and B are from the western Massif de la Hotte (A and B in Fig. 10), C is from the l'Asile region (C in Fig. 12), and E is from the Massif de la Selle (Fig. 14). For cross section D only the topography and the location of the major faults based on bathymetry and DEM is available, not the geology. .... 49

**Fig. 20:** Schematic evolutionary cross section through the l'Asile Basin, based on cross section D from **Fig. 12d**. The location of this cross section is shown on **Fig. 11**. .... 53